INTERNATIONAL JOURNAL OF MARITIME TECHNOLOGY

IJMT Vol.20 / Summer& Autumn 2024 (26-50)

Available online at: www. ijmt.ir

Predicting Sediment Transport Rate under Vegetation Cover Using Group Method of Data Handling and New Optimization Algorithms

Elham GhanbariAdivi [1*]

[1]*Associated Professor, Department of Water Science Engineering, Faculty of Agriculture, Shahrekord, Shahrekord, Iran. University- Corresponding Author: ghanbariadivi@sku.ac.ir*

ARTICLE INFO

Article History:
Received: 12 Apr 2024
Accepted: 07 Jul 2024
Available online: 13 Jul 2024

Keywords:
Sediment transport rate
Coastal regions
Forest cover
Group method of data handling
Optimization Algorithms

ABSTRACT

Developing vegetation cover is one of the practical solutions to alleviate the sediment transfer rate. Predicting the sediment transfer rate in the presence of cover vegetation is a complicated necessary issue for designers due to the complex interaction between sediments and cover vegetation. This study intends to predict the sediment transfer rate (STR) by employing soft computing models based on an experimental study. The primary innovations in this study were the introduction of new and optimized versions of the group method of data handling (GMDH) for predicting sediment transport rate, the use of a new inclusive multiple model for predicting sediment transport rate, and the investigation of the effects of various parameters on the sediment transport rate, such as vegetation cover density. This study used an inclusive multiple model (IMM) as an ensemble model to predict sediment transport in the presence of cover vegetation. Initially, the sediment transport rate was predicted using the individual GMDH models. These outputs were then used to create the final outputs by inserting them into the GMDH model as an ensemble model at the next level. The Honey Badger algorithm (HBA), the rat swarm optimization algorithm (RSOA), the sine cosine algorithm (SCA), and the particle swarm optimization algorithm (PSOA) were used to train the GMDH model. The diameter of the sediments, the diameter of the stems, the density of vegetation cover, the wave height, the wave velocity, the cover height, and the wave force were used as inputs to the models. The IMM's mean absolute error (MAE) was 0.145 m3/s, while the MAEs for GMDH-HBA, GMDH-RSOA, GMDH-SCA, GMDH-PSOA, and GMDH in the testing level were 0.176 m3/s, 0.312 m3/s, 0.367 m3/s, 0.498 m3/s, and 0.612 m3/s, respectively. The Nash–Sutcliffe coefficient (NSE) of IMM, GMDH-HBA, GMDH-RSOA, GMDH-SCA, GMDH-PSOA, and GHMDH were 0.95 0.93, 0.89, 0.86, 0.82, and 0.76, respectively. Additionally, this study demonstrated that vegetation cover decreased sediment transport rate by 90%. The overall results indicated that the IMM and GMDH-HBA models could accurately predict sediment transport rates.

1. Introduction

Prediction of sediment transport rate (STR) is one of the essential considerations in watershed management [1]. Sediment transport may cause environmental pollution. Additionally, sediment transportation may reduce the capacity of dams' reservoirs. In coastal areas, sediment transport results in disturbance in coastal residents' lives and downstream hydraulic structures [1]. Using cover vegetation that reduces flow velocity and traps sediments is an efficient solution to alleviate sediment transport rate. Sediment transport, caused by long coastal waves, adversely affects coastal hydraulic systems and structures. Controlling river ecosystems and the operation of hydraulic structures rely heavily on sediment transport rates [2]. Several strategies have been proposed to reduce sediment transport [3]. Planting vegetation is one of the most effective ways to reduce sediment transport. A vegetation cover prevents soil erosion and traps sediment. It is challenging for coastal engineers to predict sediment transport in vegetation-covered areas [4]. The presence of vegetation affects sediment transport and flow velocity [5]. The vegetation cover is an efficient solution for sediment trapping. Sediment traps are an effective way to protect rivers from sediment loads [3].

Prediction of sediment transport rate in the presence of cover vegetation is a complicated issue for managers and decision-makers in water resource management. Predicting sediment transport rate in the presence of cover vegetation is a recondite and challenging issue because of the complex interaction between sediment and cover vegetation. Many various studies have been conducted to predict the sediment transport rate (SRT) in the presence of cove vegetation so far. Wang et al. investigated the effect of vegetation density, water depth and sediment grain size on sediment transport [6]. They reported that vegetation slowed sediment transport. According to Igarashi and Tanaka (2016), integrating coastal forests and embankments reduced wave force by up to 80% compared to structural methods.

Chen et al. examined the sediment transport rate in a bare mudflat and a mangrove stand and reported that vegetation altered the flow rate [7]. Permatasari et al. investigated the correlation between mangrove density and sediment transport. There was a negative correlation between mangrove density and sediment transport [8]. Parnak et al. investigated the effect of rigid and flexible vegetation covers on the sediment transport rate. They reported that vegetation cover could significantly reduce the sediment transport rate by 70% [9].

According to Mu et al., the basal stem covers drastically reduced the transport capacity of overland flows [10]. Kusumoto et al., reported a reduction in sediment transport due to coastal forest cover [11]. As per Sun et al., ecological restoration affected sedimentary delivery [12].

The precise design of vegetation cover for sediment trapping is a complicated issue. As a result, one of the primary responsibilities of hydraulic engineers is to forecast sediment transport in the presence of vegetation cover ([1]). However, powerful models are required to make this prediction. Although numerical models can be applied to predict the sediment transport rate (SRT), using them involves solving complicated equations ([1]). Furthermore, experimental equations suggested for predicting sediment transport rate (STR) are not accurate enough. Soft computing models have provided strong sediment transfer rate (STR) prediction models in recent years. Table 1 presents a review of soft computing models' application for predicting the sediment transfer rate (STR). Soft computing models effectively predict the sediment transfer rate due to their high accuracy, low computing time, and ease of use [13].

Previous studies used soft computing models to predict the sediment transfer rate (STR) ignored the effect of cover vegetation. In addition, using individual models is one of the shortcomings of the former studies since individual models have some disadvantages besides advantages. Using ensemble models based on outputs of individual models may enhance final output accuracy [14]. Predicting the sediment transfer rate (STR) in the presence of cover vegetation using soft computing models assists watershed managers in water resource management and controlling environmental pollutants.

According to table 1, the artificial neural network is one of the feasible models for the sediment transfer rate (STR) prediction. Various types of artificial neural networks are available. GMDH is one of the most important kinds of ANN models. The group method of data handling (GMDH) is one of the most important kinds of ANN Models.

The GMDH model operates on the self-organizing principle. The GMDH algorithm makes use of polynomial transfer functions and multiple neuronal layers. The advantages of GMDH include high speed of computation and accuracy. The GMDH has been widely used in a variety of fields, including flood susceptibility prediction [15], groundwater level prediction [16], daily river flow prediction [17], and monthly streamflow prediction [18]. Mulashani et al. used (GMDH) for permeability prediction. Results revealed a reasonable reduction in processing time and high accuracy for the GMDH [19]. Panahi et al. used the GMDH model to spatially model landslides. Optimized GMDH models performed better than a standalone GMDH model in the validation [20]. A GMDH model's advantages include high accuracy, ease of implantation, and quick computation.

Although the GMDH model is robust, robust training algorithms should be used to determine the model's weight coefficients. Additionally, advanced operator-based optimization algorithms have a high potential for adjusting the GMDH parameters.

Although previous studies used soft computing models for predicting STR, there are many research gaps. Previous studies used classical soft computing models without improving accuracy. No effort was made to develop ensemble models for predicting STR. STR was estimated via experimental studies without considering robust models in previous studies. For these reasons, soft computing models must be developed for predicting STR.

The primary objective of this research is to predict sediment transport using experimental data. The effect of vegetation on the sediment transport rate was investigated in this study, and the specifics of a comprehensive experiment examining the effect of vegetation on the sediment transport rate are presented. The developed GMDH models using the new optimization algorithm were used to predict sediment transport rates in the presence of cover vegetation. This study predicts the sediment transport rate using a variety of input parameters and demonstrates how vegetation affects sediment transport rates.

Additionally, this study presents an inclusive multiple model for ensembling the outputs of GMDH models, as ensemble models have the potential to improve the accuracy of individual models by leveraging the benefits of multiple models. By combining the outputs of multiple models within an ensemble framework, the efficiency of each individual model is increased.

As a result, the following are the novelties of the current article:

1) Novel GMDH models predict the sediment transport rate using new optimization algorithms. The new optimization algorithms were used to train the GMDH model. Thus algorithms are chosen because of high accuracy, fast computation and high flexibility.
2) A new ensemble model is proposed for predicting sediment rate, namely, the inclusive multiple model (IMM).
3) A comprehensive experimental investigation into the effect of cover vegetation on the sediment transport rate is conducted.
4) The effect of various cover vegetation layouts on the sediment transport rate is determined.
5) The effect of various inputs on the prediction of sediment transport rate is examined.

Section 2 presents the material and methods. Section 3 outlines the details of the experiment. Section 4 illustrates the discussion and results. Finally, Section 5 concludes the paper.

Table 1. Application of soft computing models for predicting STR

Authors	Description	Results
Ab. Ghani and Azamathulla ,[21]	They evaluated gene expression programming (GEP) for estimating STR.	The suggested GEP model gave accurate results compared to existing predictors.
Kitsikoudis et al., [22]	They applied an adaptive-network-based fuzzy inference system (ANFIS) for STR prediction.	They reported that the ANFIS model provided better accuracy than the empirical methods.
Ebtehaj and Bonakdari, [23]	They tested several models for estimation of STR. They compared different training algorithms for estimating STR.	They found that artificial neural network-Levenberg-Marquardt performed better than existing equations.
Ebtehaj and Bonakdari, [24]	They compared two soft computing models for STR prediction.	It was found that the extreme learning machine model performed better than the support vector machine model.
Roushanger and Ghasempour, [25]	They estimated the STR in pipes using a support vector machine (SVM).	It was found that the SVM method was superior to classical methods.
Riahi-Madvar and Seifi, [26]	They estimated STR in gravel bed rivers using two soft computing models.	It was found that the ANFIS model was superior to the ANN model.
Baniya et al., [27]	They estimated STR using the bed shear stress (τ_b), specific stream power (ω), and flow velocity (v). They investigated the potential of ANN model for predicting STR.	It was found that the ANN model was superior to all the suggested models.
Kargar et al., [28]	They compared two soft computing models for STR prediction.	They found that the neuro-fuzzy model performed better than the genetic programming model.

2. Materials and methods

Different optimization algorithms have been developed to solve different problems in recent years. A new optimization algorithm, the monarch butterfly optimization algorithm (MBOA), was introduced by Wang et al. [29]. The migration of monarch butterflies was simplified and idealized, leading to the development of the MBOA. The slime mould algorithm (SMA), proposed by Li et al. [30], is an advanced stochastic optimizer. SMA simulates slime mould's search for food by introducing weights. Wang et al. [31], introduced a new metaheuristic algorithm based on the phototaxis and Levy flights of moths, called Moth Search (MS). The Hunger Games Search (HGS) technique was proposed by Yang et al. [32]. Animals' behavioral preferences and hunger-driven activities are the basis of the proposed HGS. Ahmadianfar et al. [33], developed the Runge Kutta optimizer (RUN) to handle various optimization problems. RUN is a promising and logical way to search for global optimization based on the slope variations computed by the RUN method.

Several algorithms were presented in this study for training GMDH, including the Honey Badger Algorithm, Rat Swarm Optimization Algorithm, Sine Cosine Optimization Algorithm, and Particle Swarm Optimization Algorithm (PSOA). The algorithms selected for this research are noted for their flexibility, precision, straightforward implementation, and quick convergence rates. These characteristics were the primary factors in their selection for the study.

2.1 Structure of group method of data handling

The GMDH is similar to various types of artificial neural networks. The structure of GMDH reveals the input, hidden, and output layers [34]. The observed input variables are inserted into the input layer.

GMDH's hidden layers process the data received from the first layer. Finally, the output layer produces the

$$output = \alpha_0 + \sum_{i=1}^{d} \alpha_i in_i + \sum_{i=1}^{d}\sum_{j=1}^{d} \alpha_{ij} in_i in_j + \sum_{i=1}^{d}\sum_{j=1}^{d}\sum_{k=1}^{d} \alpha_{ijk} in_i in_j in_k \quad (1)$$

Where $output$: final output, α_0, α_i, α_{ijk}, and α_{ij}: polynomial coefficients, in_i,in_j, in_k: ith, jth, and kth input and d: number of inputs. In this research, the quadratic form of the polynomial was utilized. For example, the quadratic form for a problem with two inputs is as follows [34]:

$$output = \alpha_0 + \alpha_1 in_1 + \alpha_2 in_2 + \alpha_3 in_3^2 + \alpha_4 in_2^2 + \alpha_5 in_1 in_2 \quad (2)$$

The polynomial coefficient vector is computed as follows:

$$\alpha = \left(\beta^T \beta\right)^{-1} \beta^T OUT \quad (3a)$$

Where β: a matrix based on inputs and T: transpose.

$$\beta = \begin{bmatrix} 1 & in_1^1 & in_2^1 & in_1^1 in_2^1 & \left(in_1^1\right)^2 & \left(in_2^1\right)^2 \\ . & in_1^2 & in_2^2 & in_1^2 in_2^2 & \left(in_1^2\right)^2 & \left(in_2^2\right)^2 \\ . & . & . & . & . & . \\ . & . & . & . & . & . \\ 1 & in_1^m & in_2^m & in_1^m in_2^m & \left(in_1^m\right)^2 & \left(in_2^m\right)^2 \end{bmatrix} \quad (3b)$$

Where OUT: matrix of outputs. The following equation gives the number of neurons in the next layer (N_n):

$$N_n = \begin{pmatrix} N_{np} \\ 2 \end{pmatrix} \quad (4)$$

Where N_{np}: number of the current layers. The number of neurons in the layers is limited to a maximum value to prevent the complexity of GMDH. Users can use an equation to eliminate GMDH's redundant neurons. The neurons with lower RMSE than the ξ (selection-pressure criterion) are removed.

$$\xi = \nu \times RMSE_{\min} + (1-\upsilon) \times RMSE_{\max} \quad (5)$$

Where υ: a value between 0 and 1, $RMSE_{\max}$: the RMSE of the worst neuron, $RMSE_{\min}$: the RMSE of the best neuron . The backpropagation algorithm (BPA) is one of the methods for adjusting polynomial coefficients, although it may not have a rapid convergence. In this research, robust evolutionary algorithms were used to set the polynomial coefficients of the GMDH. Figure 1a depicts the structure of GMDH [34].

desired result. The GMDH constructs a high-order polynomial named Kolmogorov-Gabor as follows [34]:

2.2 Honey Badger Algorithm (HBA)

Hashim et al. introduced the HBA algorithm as a novel optimization technique. They evaluated HBA using a variety of engineering problems [35]. The advantages of HBA include rapid convergence, high precision, and high diversity. The HBA was chosen for the current study due to these advantages and inspired by the honey badger's life. The honey badger is attracted to honey and creates holes. They remain in holes to mate with other badgers. They climb trees to gain access to beehives and nests. One of honey badger's challenges is locating beehives. A honeyguide (a bird) assists the honey badgers to locate beehives.

Additionally, the HBs dig holes within a forty-kilometer radius to trap their prey. HBs are capable of preying on squirrels and lizards and use their sense of smell to locate prey. In the first level, the location of HBs is initialized as follows [35]:

$$HB_i = lo_i + ra_1 \times \left(up_i - lo_i\right) \quad (6)$$

Where HB_i: the location of HBs, up_i: the upper bound of decision variable, lo_i: lower bound of decision variable, and ra_1: random variable. The HBs can identify the location of prey or honey based on the intensity of the smell they receive.

$$In_i = ra_2 \times \frac{S}{4\pi di_i^2} \quad (7)$$

$$S = \left(HB_i - HB_{i+1}\right) \quad (8)$$

$$di_i = HB_{prey} - HB_i \quad (9)$$

Where HB_i: the location of ith HB, HB_{i+1}: the location of i+1th HB, ra_2; random number, and In_i: smell intensity, S: source strength, and HB_{prey}: location of prey, and di_i: distance between rye and HB. The HBs excavate holes to rest and trap prey. The location of HB following digging is calculated as follows:

$$HB_{new} = HB_{prey} + F \times \rho \times In_i \times HB_{prey} + F \times ra_3 \times \eta \times di_i \times \left|\cos\left(2\pi ra_4\right) \times \left[1 - \cos\left(2\pi ra_5\right)\right]\right| \quad (10)$$

Where HB_{prey}: prey location, F: flag (it changes direction), ra_3 and r_{a4}: random parameters, ρ: controller parameter, and η: density factor. The density factor is computed as follows:

$$\eta = Z \times \exp\left(\frac{-t}{t_{\max}}\right), t_{\max} = \max imum\left(number\right) of\left(iterations\right) \tag{11}$$

$$F = \begin{bmatrix} 1 \leftarrow if\left(r_6\right) \le 0.50 \\ -1 \leftarrow else \end{bmatrix} \tag{12}$$

Where t: number of iterations and r_6 : random number.

Additionally, HBs update their location when they follow honeyguide birds to reach beehives.

$$HB_{new} = HB_{prey} + F \times ra_7 \times \eta \times di_i \tag{13}$$

Where HB_{new} : new location of the HB after following honeyguide bird and ra_7 : random parameter. Figure 1b depicts the flowchart of the HB.

2.3 Rat Swarm Optimization algorithm (RSOA)

Dhiman et al. [36] developed the ROSA based on rat behavior. ROSA's advantages include ease of execution and a small number of random parameters. They evaluated RSOA's performance on various benchmark functions and engineering problems. The ROSA algorithm outperformed the particle swarm optimization (PSO), the genetic algorithm (GA), the gravitational search algorithm (GSA), and the multiverse optimization algorithm (MOA). Rats exhibit aggressive behavior and are constantly in search of prey. A swarm of rats will follow the superior rat, aware of its prey's location. As a result, the rats update their location following the location of the rat leader as follows:

Where $R\vec{A}$: the new location of the rat, $R\vec{A}_i\left(x\right)$: the ith location of the rat, $R\vec{A}_r\left(x\right)$: the best location of the rat, S and C: controller parameters.

$$C = \gamma - x \times \frac{\gamma}{\max_{iter}}, x = 0,.., \max_{iter} \tag{15}$$

$$S = 2.rand \tag{16}$$

Where γ : a number between [1, 5], rand: random number, and $\max_{iter}$: maximum number of iterations. Rats struggle with prey in order to hunt it. This behavior is simulated as follows:

$$\vec{R}A_i\left(x+1\right) = \left|\vec{R}A_r\left(x\right) - \vec{R}A\right| \tag{17}$$

Where $\vec{R}A_i\left(x+1\right)$: The subsequent position of the rat. Figure 1c illustrates the RSOA flowchart.

2.4 Structure of Sine Cosine Algorithm

The Sine Cosine algorithm (SCA) is a novel optimization technique based on sine and cosine trigonometric functions [37]. The SCA has several advantages, including robustness, adaptability, and a high rate of convergence [38]. Each population's solution vector represents a candidate solution. The optimal solution is chosen as the final destination. The SCA algorithm updates the solution as per the following equation:

$$S_i^{t+1} = \begin{bmatrix} S_i^t + \kappa_1 \times \sin\left(\kappa_2\right) \times \left|\kappa_3 Z_i^t - S_i^t\right| \leftarrow \kappa_4 < 0.50 \\ S_i^t + \kappa_1 \times \cos\left(\kappa_2\right) \times \left|\kappa_3 Z_i^t - S_i^t\right| \leftarrow \kappa_4 \ge 0.50 \end{bmatrix} \tag{18}$$

Where κ_1 : A parameter for controlling the balance between exploration and exploitation κ_2 : A parameter for determining the direction of solutions, κ_3 : A parameter for adjusting stochastic influence of the global best solution, and κ_4 : A parameter for determining the priority of sine function or cosine function.

$$\kappa_1 = \psi - \frac{\psi i}{I} \tag{19}$$

Where ψ : constant value, i: number of iterations, I: maximum number of iterations. Figure 1d shows the SCA flowchart.

2.5 Particle Swarm Optimization Algorithm (PSOA)

PSOA is a well-known and robust optimization algorithm that operates based on information exchange between particles. The PSO possesses a strong capacity for global problem-solving. PSO's advantages include ease of implementation and a good balance between exploration and exploitation [39]. The PSO begins by determining the positions and velocity of particles [40]. The fitness function for particles was then calculated in the following step. The optimal particle with the optimal objective function was identified. The velocity and the location of particles are updated as follows:

$$ve_i^{t+1} = \varsigma ve_i^t + \mu_1\left(P_g - p_i^t\right) + \mu_2\left(P_i^* - p_i^t\right) \tag{20}$$

$$p_i^{t+1} = p_i^t + v_i^{t+1} \tag{21}$$

Where ve_i^{t+1} : velocity of i+1th at t+1th iteration, ve_i^t : velocity of ith at iteration t, P_g : current global best solution, P_i^* : individually best solution, μ_1 and μ_2 : acceleration coefficient, p_i^t : the location of the ith particle, ς : inertia coefficient, and p_i^{t+1} : the location of a particle at t+1 iteration (Figure 1f).

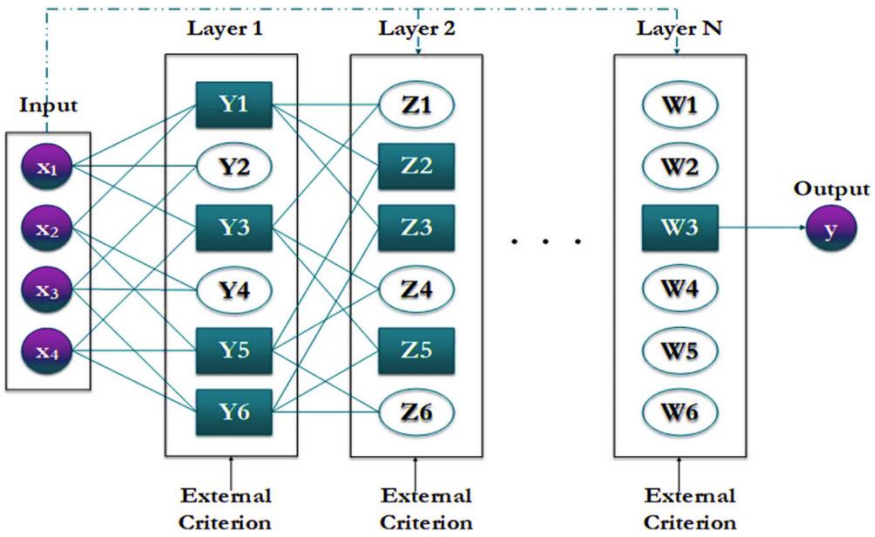

(a)

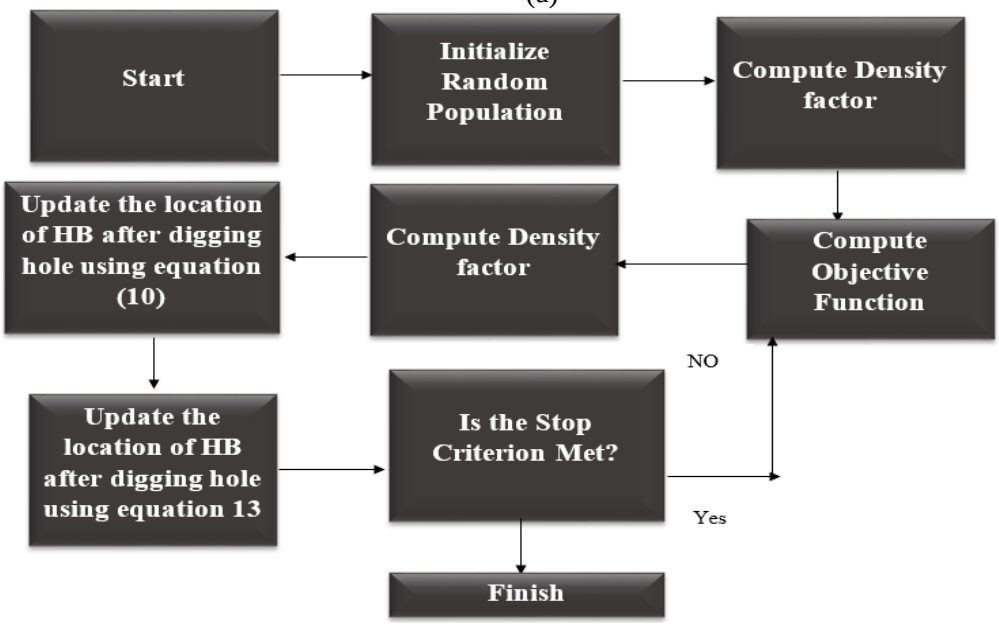

(b)

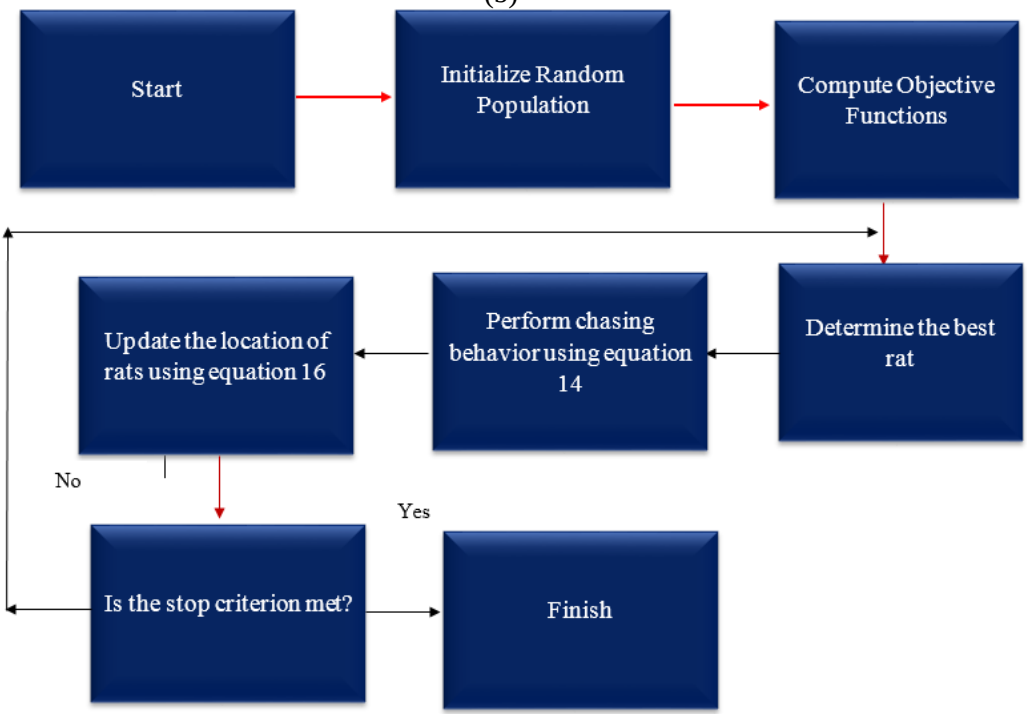

(c)

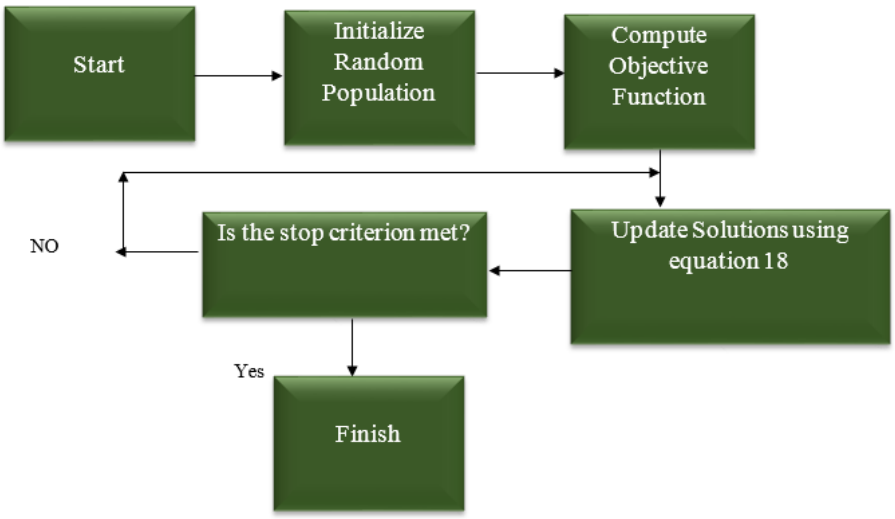

(d)

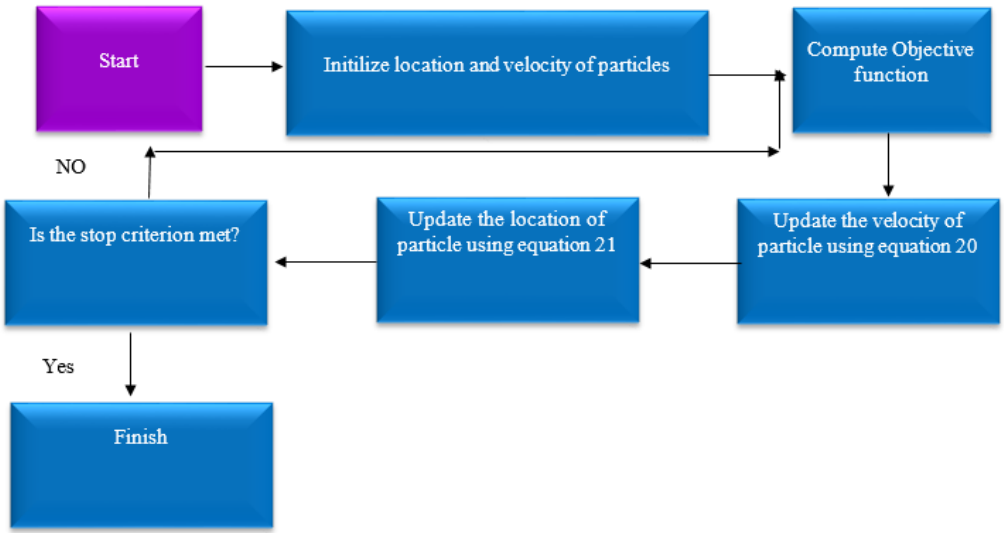

(e)

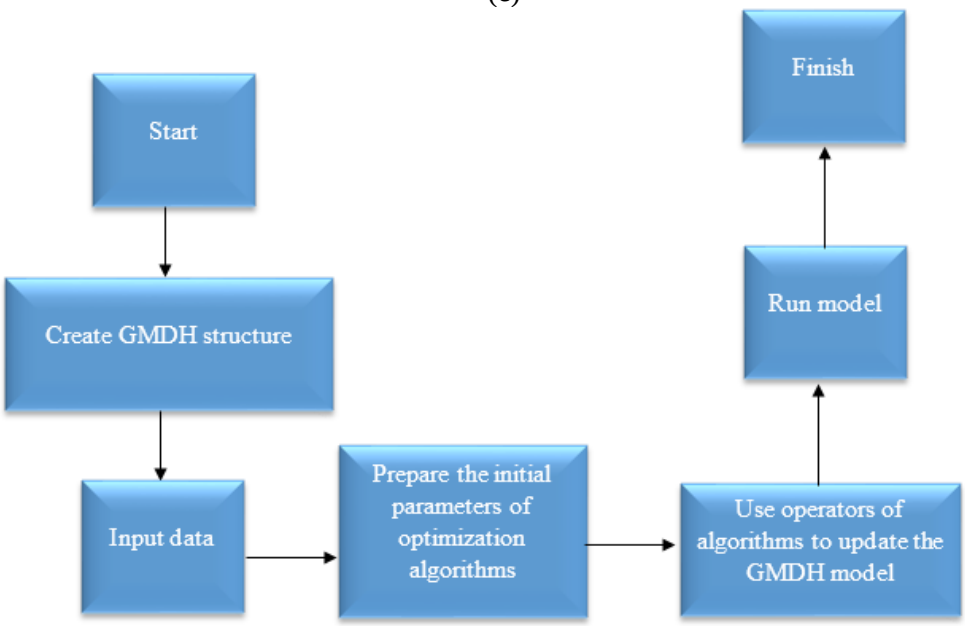

(f)

Figure 1. a: Structure of GMDH (Radiadeh and Kozlowski, 2020), b: The flowchart of HB, c: The Flowchart of RSOA, d: The SCA flowchart, e: PSO flowchart f:The structure of optimized GMDH model

2.6 GMDH integration with optimization algorithms

The HBA, SCA, RSOA, and PSOA were used in this study to compute polynomial coefficients. An optimization problem based on decision variables and an objective function was defined to determine the GMDH parameters. The following levels are considered when developing GMDH optimization algorithms:

1- Classifying the data into training and testing data.
2- Inserting the initial values of polynomial coefficients into the GMDH.
3- Running the GMDH at the training level. If the stop criterion is met, the GMDH goes to the testing level; otherwise, the GMDH connects to the optimization algorithms.
4- The polynomial coefficients have unknown values. Therefore, they are named the decision variables.
5- The initial values of polynomial coefficients are referred to as the initial population of algorithms. For instance, the location of particles represents the coefficient values of polynomials. To this end, the GMDH parameters' values are encoded to initialize the population.
6- Each agent's objective function is computed. The objective function is computed by inserting the values of the GMDH parameters into the GMDH. Following that, the RMSE is calculated as an objective function.
7- Since the location of particles, rats, HBs, and candidate solutions in SCA represents the value of decision variables, the position of agents is updated using advanced operators to obtain the new value of GMDH parameters. For example, the location of HBs was updated using HBA equations 10 and 13. Updating the location of HBs implies that the GMDH parameters' values have been updated.
8- The convergence carrion is checked. If the convergence criterion is satisfied, the process advances to level 3; if not, it proceeds to step 6 (Figure 1f).

2.7 Inclusive multiple model (IMM)

An individual model has several advantages and disadvantages. Each model has its advantages and disadvantages. For example, individual models are easily implemented to predict variables. Optimization algorithms can be coupled with them easily. Previous studies have proved that the accuracy of individual models is lower than the accuracy of ensemble models [14]. The motivation for using the IMM model is to decrease the generalization error of the prediction. GMDH models have their limitations, and producing a model with high precision is challenging. If modelers integrate multiple GMDH models, the overall precision will be boosted. This study combined the outputs of multiple hybrids and standalone GMDH models using an inclusive multiple model. First, individual GMDH, GMDH- HBA, GMDH-RSOA, and GMDH-PSOA outputs were obtained. Following that, the previous level's outputs were incorporated into a GMDH model. In fact, the second-level GMDH model is critical for assembling hybrid and standalone GMDH models. At this level, the GMDH model creates a synergy between multiple models. The GMDH generated the final output by combining the advantages of multiple models.

2.8 Case study

An increasingly favored natural method among engineers is to utilize tree stands of varying densities or hybrid Protection (tree cover and structural protection) to combat and diminish the harmful impacts of tsunami waves. This is due to their ability to generate a turbulent flow within the mass of a permeable structure, similar to a barrier [41]. This study aims to determine the role of coastal vegetation in decreasing sediment transport. For this purpose, the data used in the research by Mirzakhani et al., has been utilized, which is further described in the subsequent laboratory conditions of the mentioned research [42]. The waves examined in this article fall under the category of shallow water waves (relative depth less than 0.5). The experiments were conducted in a flume located in Shahrekord University's hydraulic laboratory. The flume's length, width, and height were 20 m, 60 cm, and 60 cm, respectively. The flume's floor and wall were constructed of metal and Plexiglas, respectively. The flume used is depicted in Figures 2a and Figure2b. Experiments were conducted in a flume at an 8.6 m distance. This interval was divided longitudinally into three sections, 2m, 3m, and 3.6m to construct the water tank, shore, and downstream. Based on field reports, Palm tree is one of the resistive trees against the destructive effects of waves. Accordingly, rigid plastic cylinders were used to simulate cover vegetation on the scale of 1:50 to match the model against the reality. Table 2 shows the details of the experiments. The experiment's water distribution system consists of a piping network, a pumping system, and a water tank. The beach was constructed using a galvanized sheet measuring 1 m in length, 0.59 m in width, and 6 mm in thickness. The beach was constructed on a fixed and horizontal slope.

The tank at the start of the desired area was created using a Plexiglas plate. Afterward, the sliding gate was placed 2 m away from the Plexiglas wall. The initial height of the input waves was simulated using a 50:1 scale following the height of the tsunami wave, which was between 3 and 15 meters high. The tank was topped off with water to the desired depth. The gate was then quickly opened, and the height of the broken wave was determined at the shore. Two gates were used in this experiment. The upstream gate applies to generate waves. The downstream flume valve balances the water level. Along with the ADV (Acoustic Doppler velocimeter), a video camera operating at a frame rate of 30 frames per second was used to record the wave characteristics at the refraction moment. ADV was

used to record the wave velocity. The camera was positioned against the flume's wall and adjusted to include the beach in the frame. The constant sill height (Y) was 6.5 cm. A dynamometer connected to the transverse part of the flume was applied to record the wave force crashed onto the beach, with and without cover vegetation. Following preliminary experiments, it was determined that three waves with heights of 25.6 cm, 39.5 cm, and 47 cm behind the upstream gate generate waves with heights of 6, 9, and 12 cm on the beach following the gate. The wave heights of 6, 9, and 12 cm correspond to the wave heights at the refraction moment. The sediment transport rate depends on the wave heights at the refraction moment [1]. The details of the forest cover are shown in Table 2 and Figure 3a. Two triangular and rectangular forest cover layouts were used to examine the effect of different vegetation layouts on sediment transport. The rectangular and triangular layouts for the vegetation cover density VCD =273 (number/m^2) and VCD =66 (number/m^2) are shown in Figures 3b and 3c. Sediment transport rates are depicted in Figure 3d. Furthermore, Figure 3e illustrates the heights produced at the refraction moment for the VCD=273 sample.

Sand particles ranging in size from 0.25 to 0.59 mm with an average diameter of 0.35 mm were used as sedimentary porous materials in this study. The wave velocity values in the conducted experiments depend on the wave height under consideration and the laboratory conditions taken into account, including the speed of the wave-generating gate opening. Averagely the wave velocity varies between 1-2 meters per second. Moreover, IMM, hybrid, and standalone GMDH models were used to predict sediment transport rates.

(a)

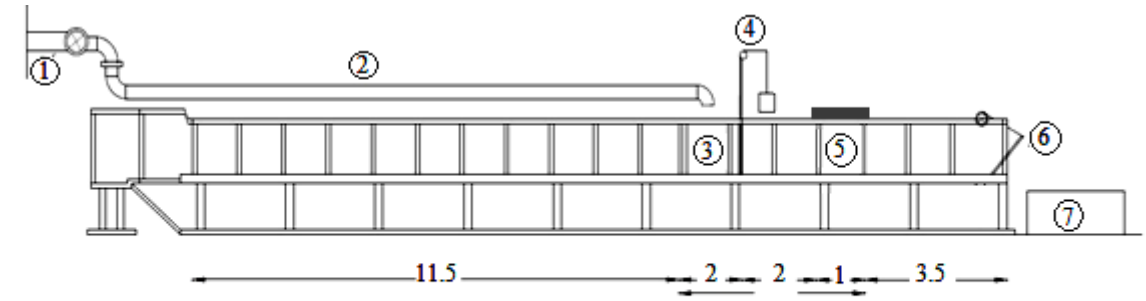

All dimensions are in meters

1- The main water pipe 2- Inlet water pipe to the wave tank 3-Wave head supply tank 4-Sliding gate
5- Movable frame (with knife edge support) 6-End valve 7-Flow drainage tank

Figure 2. a: Details of used Flume, and b: The structure of flume

Table 2. The details of layout of vegetation cover

Longitudinal and transverse distance	Number of rows	Density (number /m^2)	Number of stems		Configuration (Rectangular)	Configuration (Triangular)
			Rectangularity	Triangular		
20×20	4	24	12	10	R_1	T_1
	3	18	9	8		
	2	12	6	5		
15×15	5	40	20	18	R_2	T_2
	4	32	16	14		
	3	24	12	11		
	2	16	8	7		
10×10	7	77	35	31	R_3	T_3
	6	66	30	27		
	4	44	20	18		
	3	33	15	14		
5×5	13	273	117	111	R_4	T_4
	10	210	90	85		
	7	147	63	60		
	4	84	36	34		

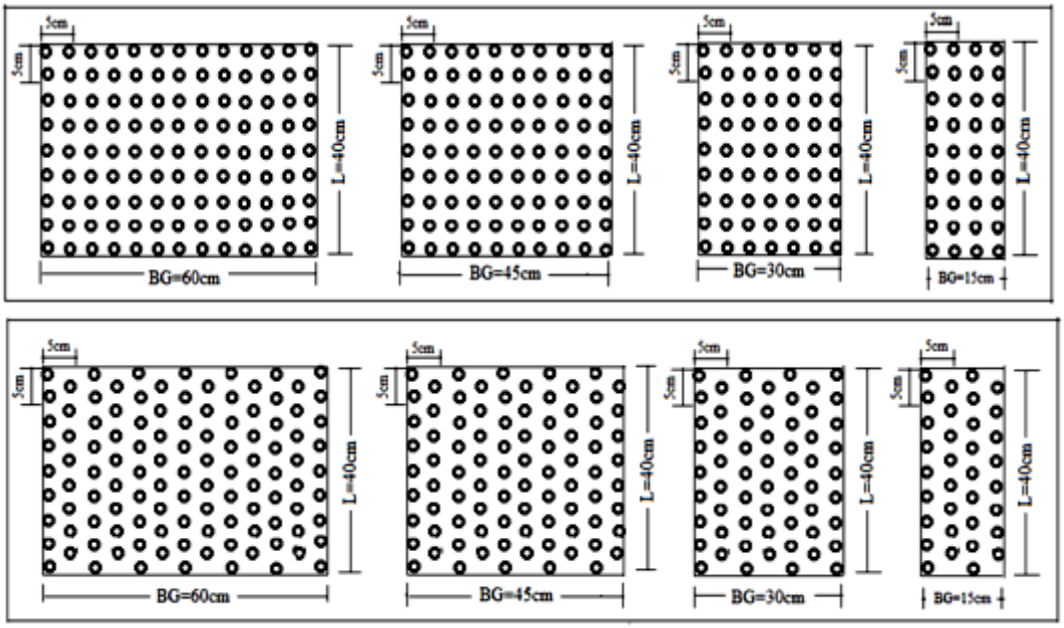

(a)

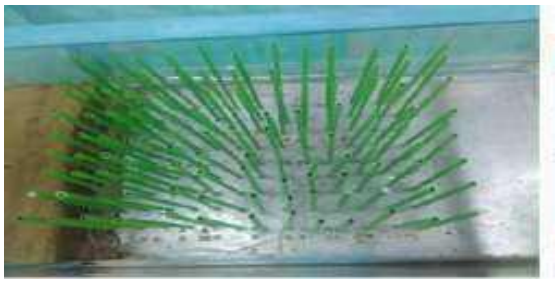

(b)

(c)

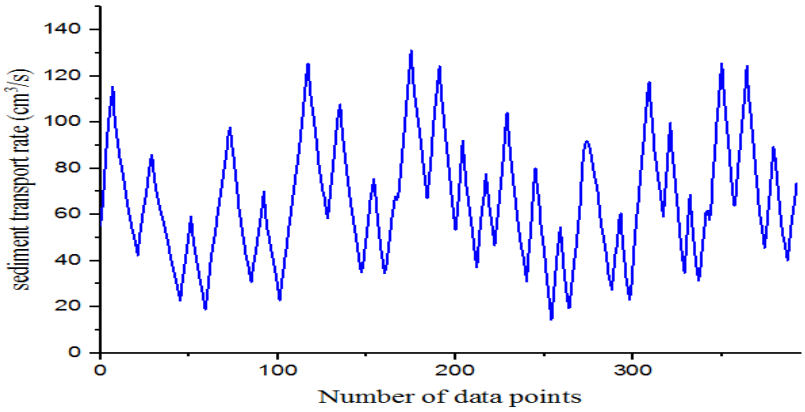

(d)

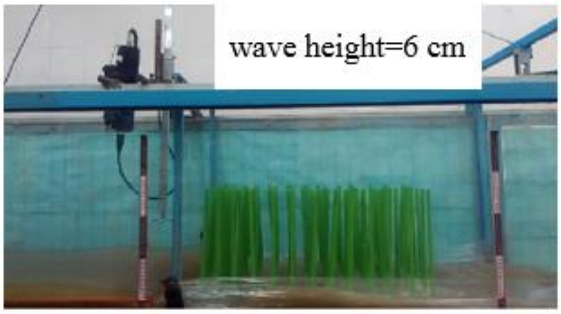

e

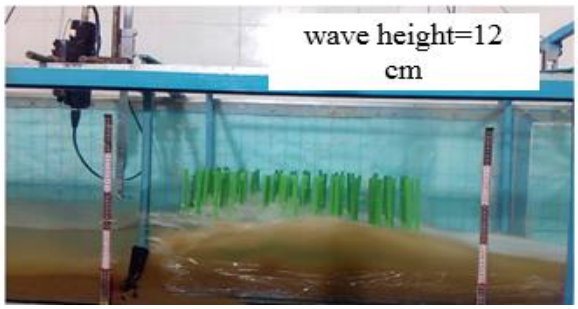

e

Figure 3. a: Configurations of forest covers, b: rectangular layouts for the vegetation cover density (VCD) =273, c: Triangular and triangular layouts for the vegetation cover density (VCD) =273 and d: sediment transport data points, e: produced waves at the refraction moment

According to Jalil-Masir et al. ([1, 43]), the sediment transport rate was determined by a variety of factors, including the diameter of the sediments, the diameter of the stems, the cover density, the initial height of the wave, the wave velocity, the cover height, and the wave force. The input parameters in Table 3 were used to predict the sediment transport rate under the specified vegetation conditions. The sediment transport rate was predicted in this study using 393 data sets.

In this study, the following levels were considered for the experiment:

1- The sand was used as the bed material for the flume.
2- The nets were placed after the sediment drain gate for gathering sediments.
3- The upstream reservoir was filled with water.
4- The camera and velocity meter were located on the beach for recording information.
5- A pulley and weight system were applied to open the upstream gate abruptly.
6- The solitary wave was generated based on an abrupt opening gate.
7- The camera and velocity meter recorded the wave height and velocity in the refraction point.
8- The sediment samples were gathered downstream.
9- The samples were stored in the laboratory at 25 °C for 36 h.
10- A sensitive balance was used to determine the weights of samples.

Table 3. The used inputs for predicting sediment transport rate

Parameter	Average	Maximum	Minimum	Standard deviation
Number of experiments: 393 and number of data:393				
height at the refraction moment (H_W) (cm) (height wave after gate)	9	12	6	2.64
Vegetation cover density (number /m^2) (DS)	73.33	273	12	75.44
Wave force (F) (unit:N)	51.66	190.29	12.86	33.50
D_{50} (mm)	0.33	0.35	0.30	0.26
Height of vegetation cover (h_v) (cm)	32	35	30	5.73
cover stem diameter D (cm)	0.55	0.90	0.30	0.40
Velocity (m/s) V_W	1.46	1.53	1.34	0.03

The following indices were used as follows [44]:

1- Root mean square error

$$RMSE=\sqrt{\frac{\sum_{i=1}^{N}\left(RST_{ob}-RST_{es}\right)^2}{N}} \quad (22)$$

2- Mean absolute error (MAE)

$$MAE=\frac{1}{N}\sum_{i=1}^{N}\left|RST_{ob}-RST_{es}\right| \quad (23)$$

3- Percentage of bias (PBIAS)

$$PBIAS=\frac{\sum_{i=1}^{N}\left(RST_{es}-RST_{ob}\right)}{\sum_{i=1}^{N}RST_{ob}} \quad (24)$$

4- Nash–Sutcliffe efficiency

$$NSE=1-\frac{\sum_{i=1}^{N}\left(RST_{es}-RST_{ob}\right)^2}{\sum_{i=1}^{N}\left(RST_{ob}-\overline{RST}_{ob}\right)^2} \quad (25)$$

5- Fraction of standard deviation (FSD):

$$FSD\left(RST_{es},RST_{ob}\right)=2*\frac{\left|SD(RST_{es})-SD\left(RST_{ob}\right)\right|}{SD\left(RST_{es}\right)+SD\left(RST_{ob}\right)} \quad (26)$$

Where RST: rate of sediment transport, $SD(RST_{es})$ SD: standard deviation of estimated RST, $SD\left(RST_{ob}\right)$: standard deviation of observed RST, RST_{obs}: observed RST, RST_{es}: estimated RST, $\overline{RST}_{ob}$: Average observed RST, N: number of data.

3. Results and discussion

3.1 Training and testing level size selection

The various data sizes for the individual models were tested and depicted in Figure 4 to determine the optimal

size for simulations at the training and testing levels. As illustrated in Figure 4, the optimal training and testing data sizes for all models were 70% and 30%, respectively, because the objective function (RMSE) had the smallest values for these data sizes. For example, using the GMDH model, the objective function for 50%, 55%, 60%, 65%, 70%, and 80% of data was 1.05, 0.91, 0.967, 0.845, 0.800, and 0.833, respectively. As a result, 70% and 30% of the data for the training and testing levels were chosen in this study.

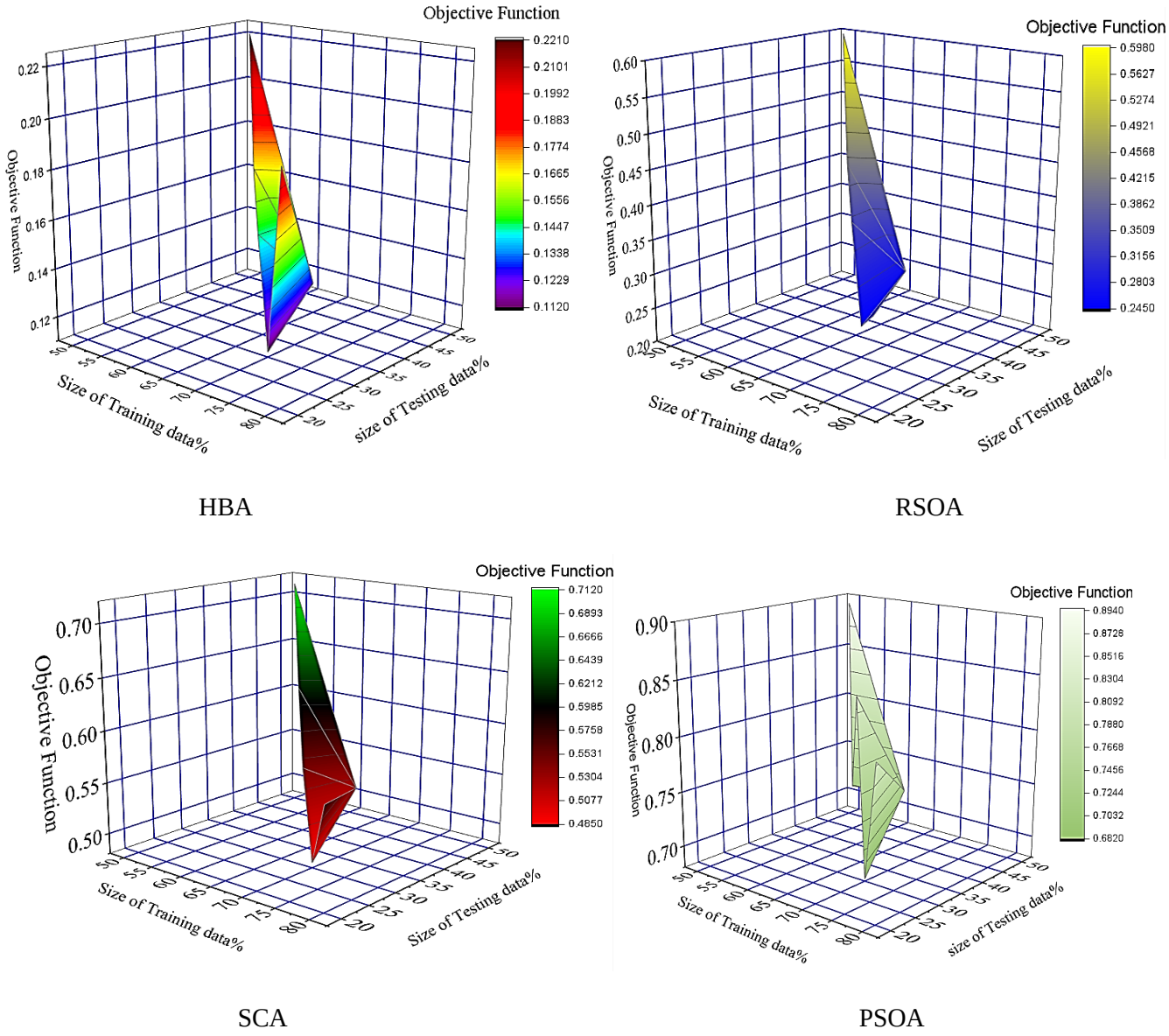

Figure 4. The choice of best size for data

3.2 Best value determination for random parameters

Each optimization algorithm has random parameters (RPs). It is critical to determine the optimal value of RPs in order to achieve the best results when using optimization algorithms. The objective function varies with different values of RP, as shown in Table 3. The HBA population ranged in size from 50 to 200. It was discovered that the optimal population size was 100 because it resulted in the smallest objective function value (RMSE). The maximum number of HBA iterations was variable between 40 and 160. The best value of a maximum number of HBA iterations was 80 because it resulted in the lowest objective function value (RMSE). The population size of RSOA varied between 50 and 200. The best value for the RSOA population size was 100. At the maximum number of iterations =100, the RSOA achieved the lowest value of the objective function. The values of other algorithm parameters were determined via a similar process. While the value of one parameter was varied, the values of the other parameters remained constant.

Table 4. The sensitivity analysis of random parameters of algorithms

(Population size: POS, Objective Function: OBFU, the maximum number of iterations: MANI)

HBA

POS	OBFU	MANI	OBFU
50	0.167	40	0.169
100	0.123	80	0.134
150	0.190	120	0.187
200	0.198	160	0.98

RSOA

POS	OBFU	MANI	OBFU
50	0.345	50	0.367
100	0.267	100	0.266
150	0.298	150	0.399
200	0.312	200	0.412

SCA

POS	OBFU	Maximum number of iterations	OBFU	κ_2	OBFU	κ_2	OBFU
50	0.345	100	0.367	$\pi/3$	0.389	0.60	0.376
100	0.267	200	0.266	$2\pi/3$	0.276	0.80	0.265
150	0.298	300	0.399	$3\pi/3$	0.265	1.00	0.298
200	0.312	400	0.412	$4\pi/3$	0.291	1.2	0.322

3.3 Best input scenario selection

Eight input scenarios were considered in this section to determine the effect of inputs on outputs. The input scenario is defined in Table 5. Figure 5 illustrates the objective function's (RMSE) value for various input scenarios and models. The RMSE of GMDH-HBA based on input scenario (1) -(8) were 0.123 cm^3/s, 0.233 cm^3/s, 0.322 cm^3/s, 0.412 cm^3/s, 0.523 cm^3/s, 0.612 cm^3/s, 0.789 cm^3/s, and 0.812 cm^3/s, respectively. It was discovered that utilizing all input variables resulted in the best results. By excluding the wave height at the refraction moment from the input combination, the RMSE was increased by 84%. Additionally, removing the cover height from the input combination increased the RMSE by 47%. Thus, the highest and lowest significance values for the GMDH-HBA were the wave height at the refraction moment and the cover height, respectively.

The RMSE of GMDH-RSOA based on the input scenarios (1) -(8) were 0.267 cm^3/s, 0.278 cm3/s, 0.392 cm^3/s, 0.567 cm^3/s, 0.612 cm^3/s, 0.823 cm^3/s, 0.901 cm^3/s, 0.911 cm^3/s, respectively. By removing the wave height from the input combination, the RMSE was increased by 70%. The second critical parameter for the GMDH-RSOA was the wave velocity. Other models' results indicated that the most important parameters for predicting sediment transport rate were wave height, wave velocity, density cover, and D_{50}.

3.4 Model accuracy evaluation

The first input scenario was used to run all models in this section. In the preceding section, the first input scenario produced the best results. Figure 6 illustrates radar plots to assess the accuracy of models. The accuracy of models based on PBIAS is compared in Figure 6a. The IMM had a PBIAS of 8%, whereas the GMDH-HBA, GMDH-RSOA, GMDH-SCA, GMDH-PSO, and GMDH at the training level had PBIASs of 12, 16, 22, 27, and 33%, respectively. According to the outputs, the IMM and GMDH based on PBIAS produced the best and worst results, respectively. PBIAS of GMDH-HBA was 15% at the testing level. The HBA outperformed the other optimization algorithms. The values of the models' NSE are shown in Figure 6b. The IMM had an NSE of 0.98 at the training level, whereas the GMDH-HBA, GMDH-RSOA, GMDH-SCA, GMDH-PSO, and GMDH had NSEs of 0.97, 0.94, 0.87, 0.85, and 0.80, respectively. The IMM, GMDH-HBA, and GMDH-RSOA demonstrated the highest degree of accuracy at the testing level. Figure 6c illustrates the FSD values for the various models. The FSD of IMM was 1.11, while the FSDs of GMDH-HBA, GMDH-RSOA, GMDH-SCA, GMDH-PSO, and GMDH were 0.23, 0.67, 0.85, 1, and 1.22, respectively. The accuracy of the results indicated that the GMDH-HBA performed better than the GMDH-RSOA, GMDH-PSOA, GMDH-SCA, and GMDH. Figure 6d illustrates the MAE values for the various models. The IMM decreased the MAE of the

IMM models GMDH-HBA, GMDH-RSOA, GMDH-SCA, GMDH-PSO, and GMDH by 24%, 58%, 58%, 75%, and 80%, respectively, at the training level. The IMM was found to have the lowest MAE at the testing level. This section's findings indicated that the IMM and GMDH-HBA had the highest accuracy. The IMM operates based on the possibility of multiple independent models. When an IMM model takes advantage of the multiple individual models, the IMM model's accuracy increases significantly. The HBA is equipped with advanced operators. The HBA solutions can be updated using equations 10 and 13. This enables the HBA to circumvent local solutions. Additionally, these equations enable the HBA to improve the solution's quality. The IMM model in this study performed better than other models. Jalil-Masir et al. used regression models and the same data points for predicting STR. A regression model and the data points of the current study were used by Jalil-Masir et al. (to estimate STR. They reported the R^2 value of 0.84 for the regression model. Thus, the IMM of the current study performed better than the regression models [1].

Table 5. The defined input scenarios for the models

1	H (W), V(W), D(S), F, D_{50}, h(v), D
2	H (W), V(W), D(S), F, $D_{(50)}$, D
3	H (W), V(W), D(S), F, $D_{(50)}$, h(v)
4	H (W), V(W), D(S), $D_{(50)}$, h(v) , D
5	H (W), V(W), D(S), F, h(v), D
6	H (W), V(W), F, $D_{(50)}$, h(v), D
7	H (W), D(S), F, $D_{(50)}$, h(v), D
8	V(W), D(S), F, $D_{(50)}$, h(v), D

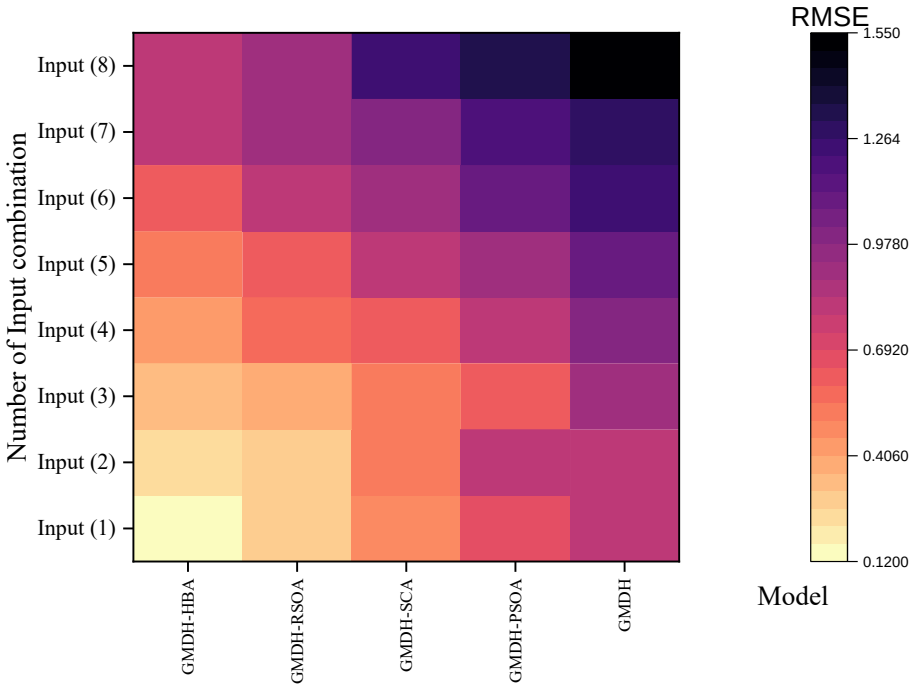

Figure 5. The computed RMSE for different input scenarios and models

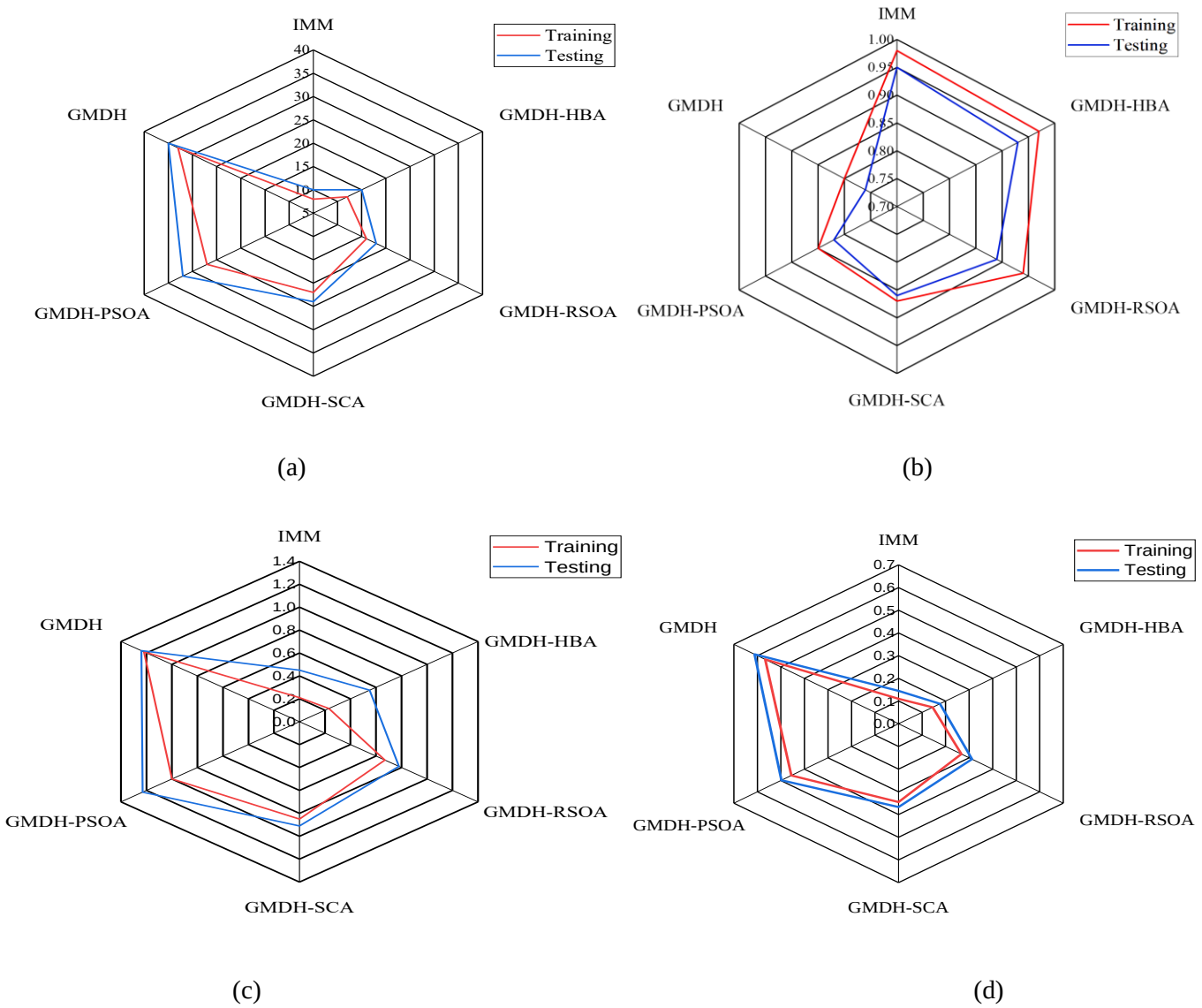

Figure 6. Radar plots base for a: PBIAS, b: NSE, c: FSD, and d: MAE

For the reasons stated previously, the HBA outperformed the other algorithms. While back propagation was used to train the GMDH, optimization algorithms significantly improved its accuracy. The residuals histogram is shown in Figure 7. The histogram of the residual for the IMM model is shown in Figure 7a. In this Figure, 308 and 73 data points fall within the -1 and 1 bin centers, respectively. Other bin centers receive a small number of data. The histogram of the residual for the GMDH-HBA model is shown in Figure 7b. The residual of 263 data points is 2.5. Additionally, 112 and 7 data points fall in the -2.5 and -7.5 bin centers, respectively. The residual histogram for the GMDH-RSOA model is shown in Figure 7c.
The residuals for the 301, 60, 6, and 5 data points are 2.5, -2.5, -7.5, -12.5, and -17.5, respectively. The residual histogram for the GMDH-SCA model is depicted in Figure 7d. The residuals for 300, 53, 15, 7, and 5 data points are 2.5, -2.5, -7.5, -12.5, and -17.5, respectively. The histogram of the residual for the GMDH-PSOA model is shown in Figure 7e. The residual distribution of 272, 73, 15, 9, and 5 data points is 2.5, -2.5, -7.5, -12.5, and -17.5, respectively. Other data points' residuals fall into the other center bins. Finally, Figure 7f depicts the histogram of GMDH residuals. The residuals for 309, 25, 17, 12, 8, 5, and 2 data points are 2.5, -2.5, -7.5, -12.5, -17.5, -22.5, and -27.5, respectively. Other data points' residuals fall into the other center bins. Some of the outputs of GMDH had residuals of >-42.5. In general, the IMM and GMDH outperformed the other models in this section.
The boxplots for the models are shown in Figure 7g. The median of the observed data, IMM, GMDH-HBA, GMDH-RSOA, GMDH-SCA, GMDH-PSOA, and GMDH were 58.5 cm^3/s, 58.5 cm^3/s, 58.5 cm^3/s, 63 cm^3/s, 63 cm^3/s, 63 and 63 cm^3/s, respectively. The mean of the observed data, IMM, GMDH-HBA, GMDH-RSOA, GMDH-SCA, GMDH-PSOA, and GMDH was 67.0 cm^3/s, 67.0 cm^3, 66.7 cm^3/s, 68.7 cm^3/s, 69.0 cm^3/s, 69.7 cm^3/s, and 69.8 cm^3/s, respectively. It was discovered that the IMM and observed data had a high degree of correspondence.

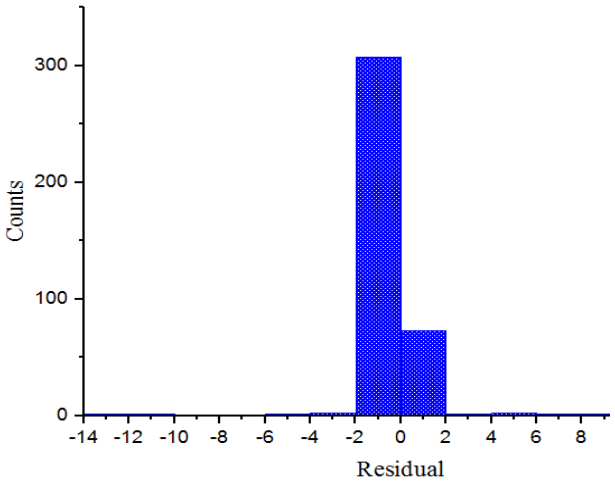

(a)

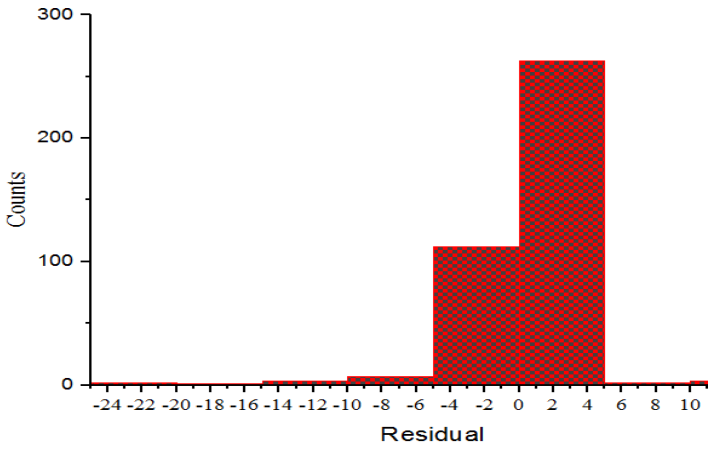

(b)

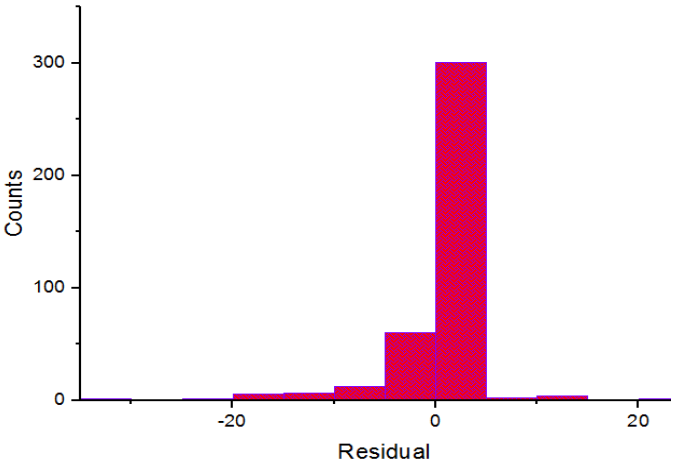

(c)

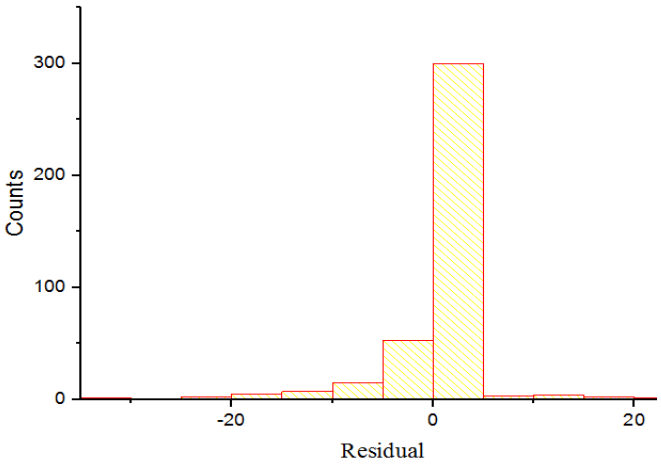

(d)

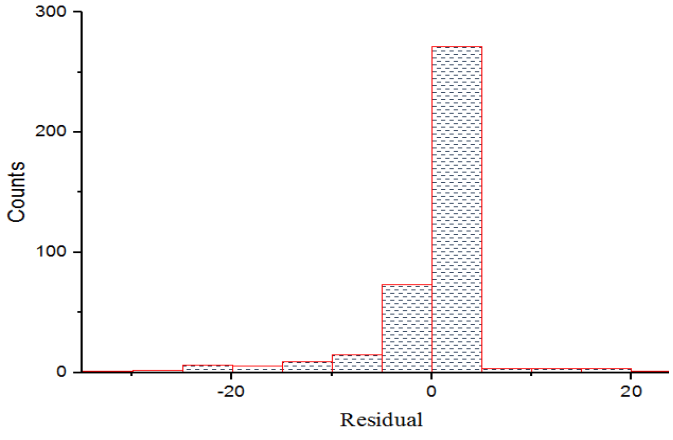

(e)

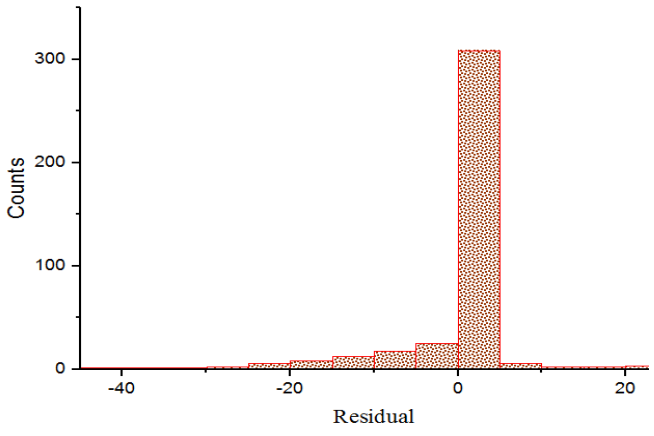

(f)

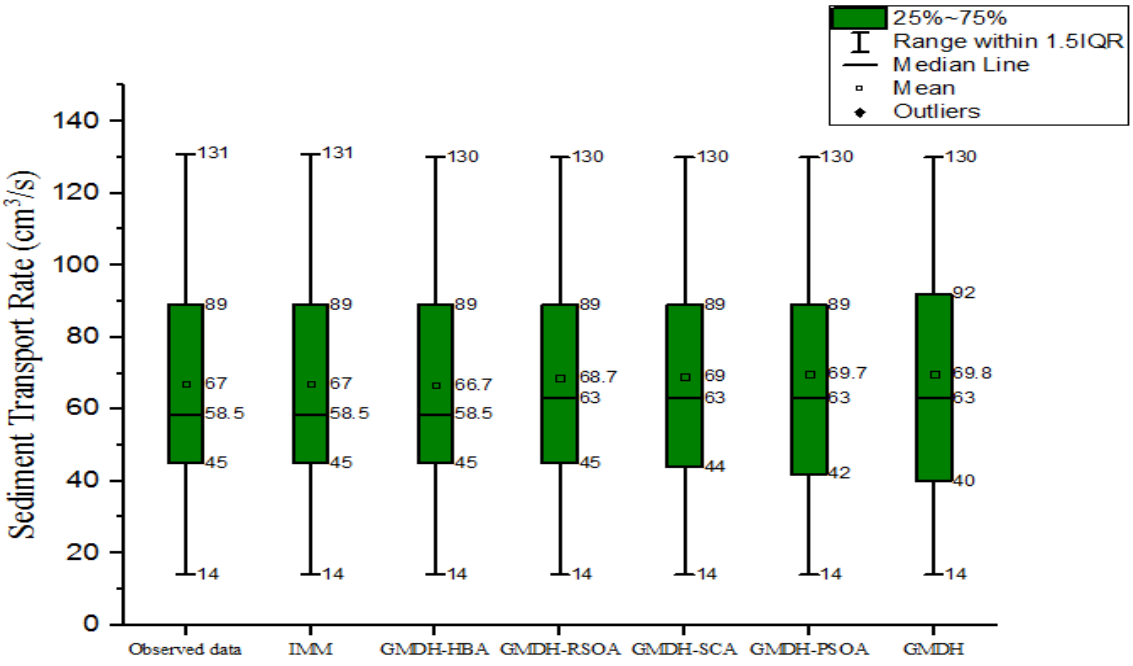

g

Figure 7. The histogram of residual values of models for a: IMM, b: GMDH-HBA, c: GMDH-RSOA, d: GMDH-SCA, e: GMDH-PSOA, f: GMDH, and g: The boxplots of models for estimating STR

The density scatterplots are depicted in Figure 8. When many data points cannot be clearly identified, the density scatterplot is advantageous. A density scatterplot determines the density of data in a given area. The density scatterplots for the IMM, GMDH-HBA, GMDH-RSOA, GMDH-SCA, GMDH-PSOA, and GMDH are shown in Figures 8a, 8b, 8c, 8d, 8e, and 8f, respectively. IMM, GMDH-HBA, GMDH-RSOA, GMDH-SCA, GMDH-PSOA, and GMDH had R^2 values of 0.9963, 0.9887, 0.9741, 0.9669, 0.9443, and 0.9267, respectively. The density values indicate that a substantial amount of data was located between 43.80 cm^3 and 73.70 cm^3, implying that this interval contains the highest density for all models. In this region, a large number of data points overlap. All models exhibit a low density value at the upper and lower limits of the sediment transport rate.

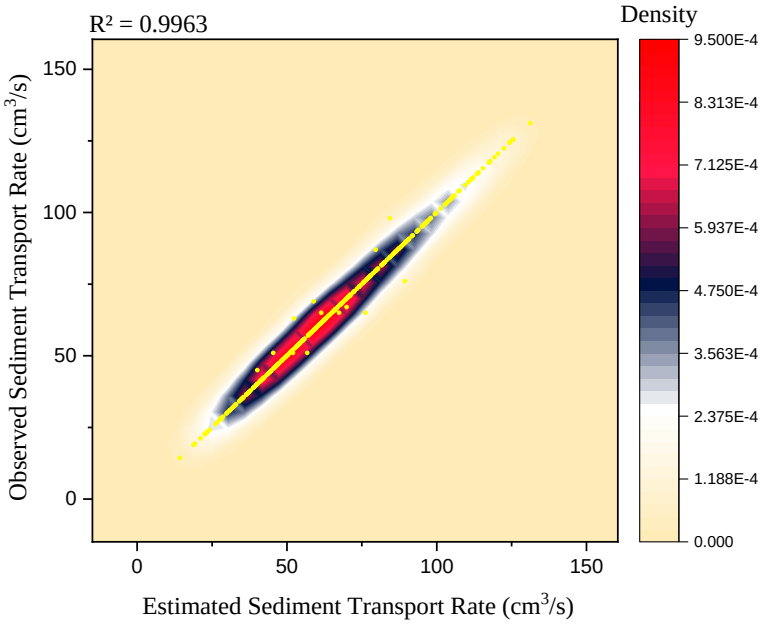

IMM

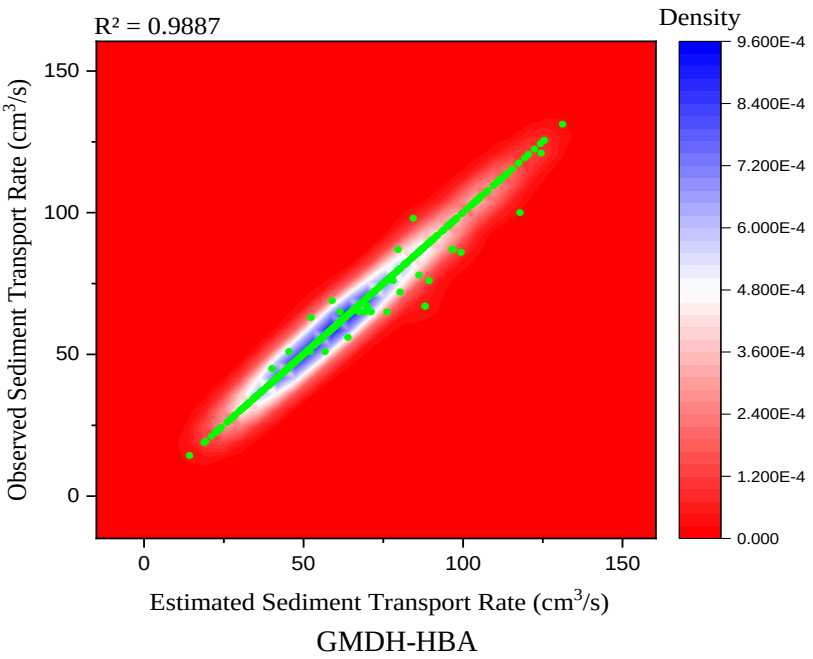

GMDH-HBA

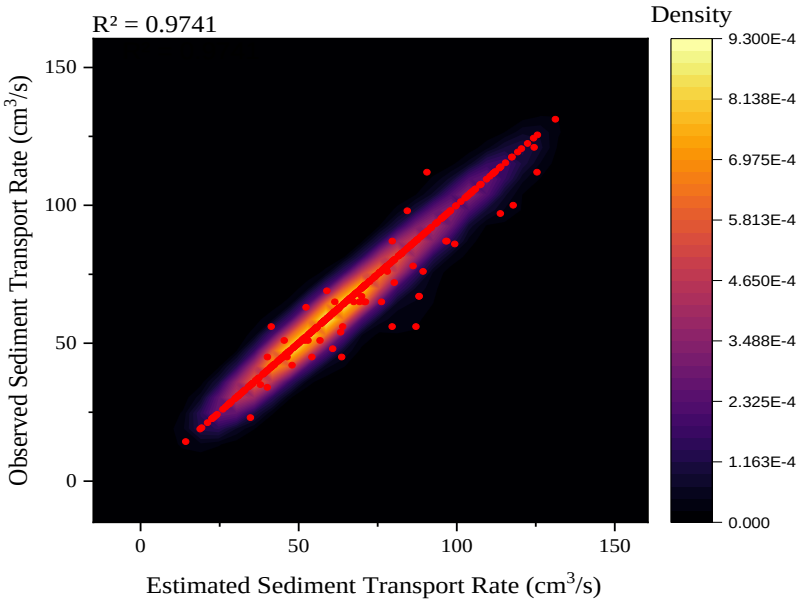

GMDH-RSOA

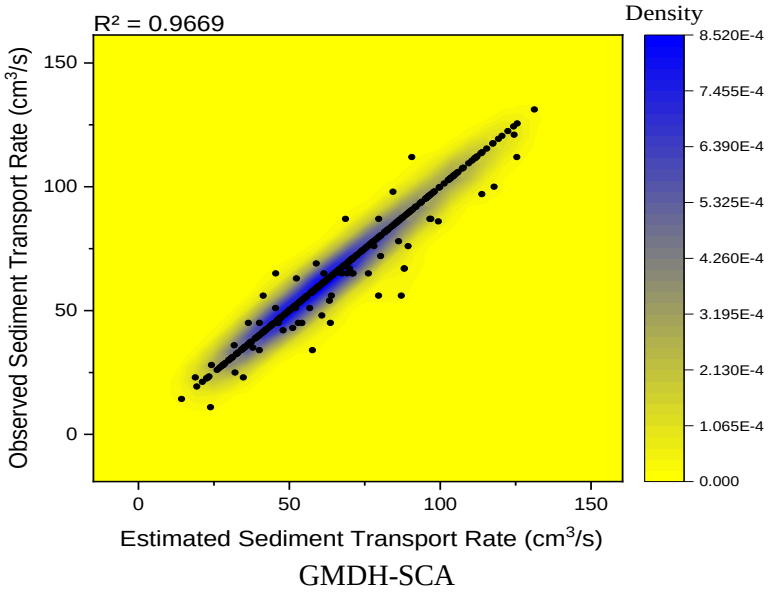

GMDH-SCA

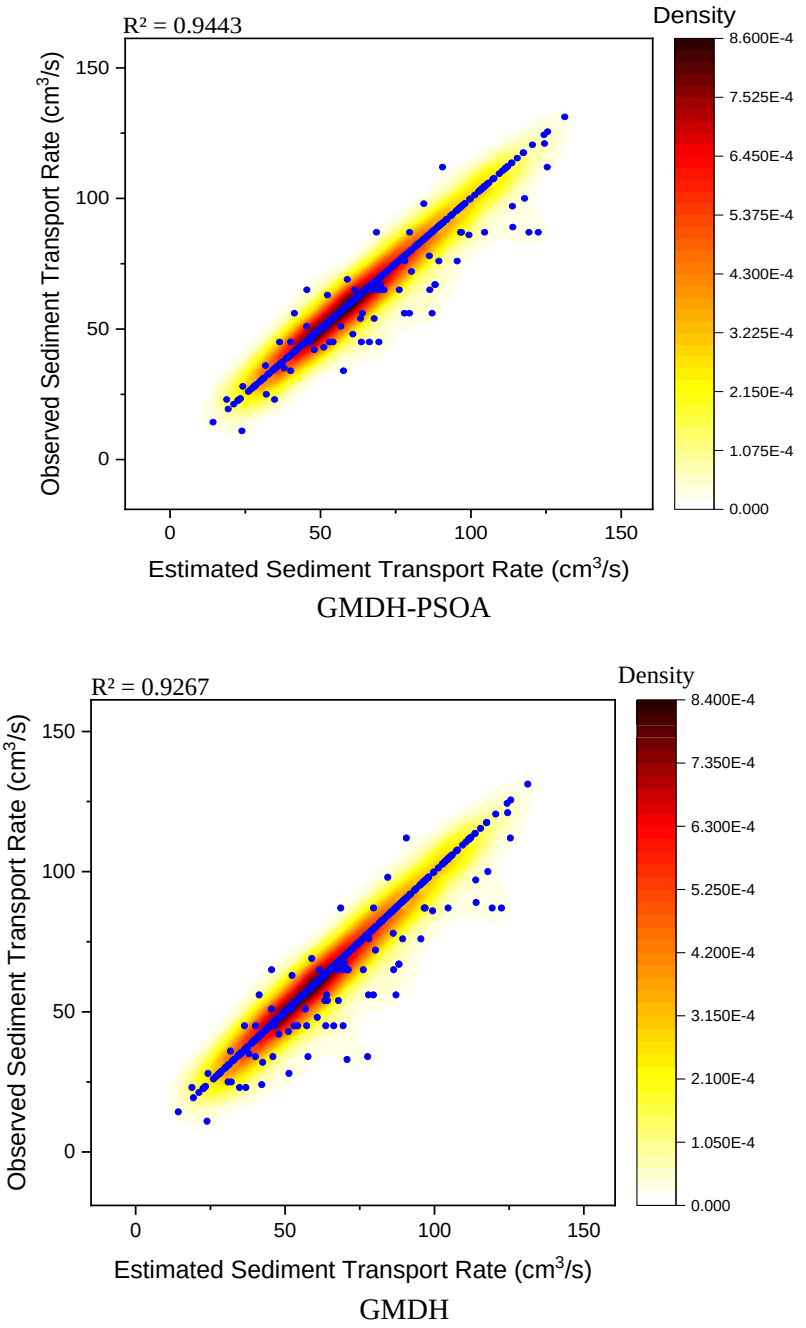

Figure 8. The heat scatter plots of models

3.5 Further discussion

This section examined the effect of various parameters on sediment transport rate. The vegetation cover was used in this study to conduct the experiments. Vegetation cover reduces sediment transport and wave velocity. Figure 9a illustrates the velocity and height wave variations for different vegetation cover densities (VCD) using a rectangular layout. When the VCD value increases, the wave velocity should be increased to maintain a constant height wave. This indicates that utilizing forest cover effectively reduces the height wave at the refraction moment. For example, at VCD =12 and wave height=6 cm, the rectangular layout produces a wave velocity of 1.34 m/s. For maintaining a constant height of 6 cm at VCD =44 and VCD =210, the wave velocity should be increased from 1.34 (VCD =12) to 1.40 (VCD =44) m/s and 1.34 (VCD =12) to 1.42 (VCD =210) m/s, respectively. Figure 10b demonstrates the velocity and height waves variations for three VCD s of 12, 44, and 210 based on a triangular layout.

The triangular layout results also indicated that increasing the VCD decreased the wave height. Figures 9a and 9b demonstrated that the triangular layout was more effective at reducing height wave than the rectangular layout. For example, at VCD =12 and wave height=6 cm, the rectangular layout produces a wave velocity of 1.34 m/s, while the triangular layout

produces a wave velocity of 1.38 m/s. The velocity should be increased from 1.34 m/s to 1.38 m/s to maintain the 6 cm height in the triangular layout. In fact, the triangular configuration is more effective at reducing wave force. As a result, it can significantly reduce wave velocity. The results of Figures 13 and 14 3 demonstrate that as wave height increases, velocity increases as well. The velocity for H=6, H=9, and H=12 cm was 1.34 m/s, 1.38 m/s, and 1.42 m/s in the rectangular layout's VCD =12. Since the triangular layout increased the drag force and cover resistance against the flow, it could significantly decrease the total sediment rate.

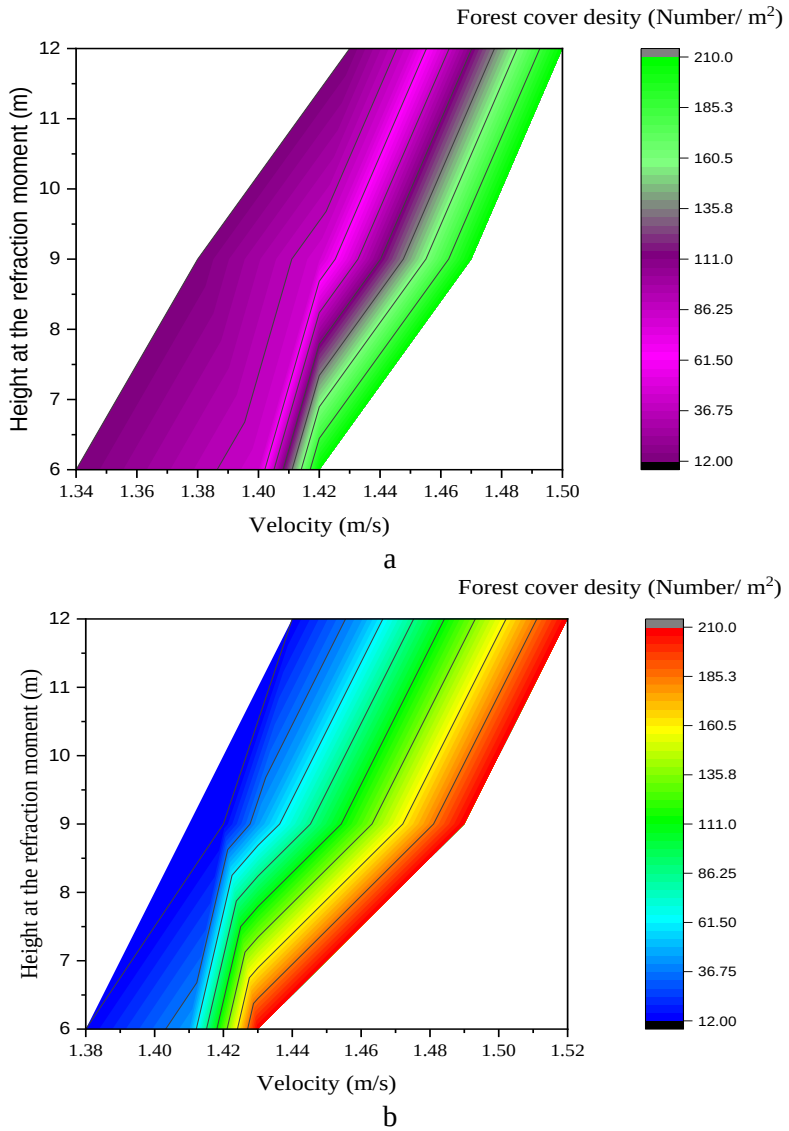

Figure 9. The investigation of height and wave velocity for different CFCs based on a: rectangular layout and b: triangular layout

Figure 10a plots the dimensionless sediment transport rate (DSTR) against the dimensionless wave height ratio (H (at the refraction moment)/Y (sill height)) for the R_1 configuration. The DSTR is calculated by dividing the mass of sediments in the presence of cover vegetation by the mass of sediments in the absence of cover vegetation. By increasing the height of the waves, the sediment transport rate is increased. For instance, when the number of rows of vegetation cover was equal to four, the DSTR for H/Y=0.65, H/Y=0.9, and H/Y=1.2 was 0.52, 0.58, and 0.61, respectively. NRVC is a numerical value that indicates the number of rows of vegetation cover. DSTR versus H/Y plots for R2, R3, and R4 configurations are shown in Figures 10b, 10c, and 10d, respectively. DSTR decreased as the number of rows of forest cover increased in these figures. For example, in the H/Y=0.65 configuration of R_4, the DSTR of NRVC=12, NRVC=10, NRVC=7, and NRVC=4 was 0.14, 0.20, 0.30, and 0.39, respectively. The DSTR versus the H/Y for the T1 configuration is depicted in Figure 10e.

Increase in H/Y resulted in an increase in DSTR in this Figure. For instance, the DSTR for H/Y=0.65, H/Y=0.9, and H/Y=1.2 was 0.42, 0.50, and 0.55 when the number of rows of vegetation cover was equal to four. The DSTR versus the H/Y is depicted in Figures 10f, 10g, and 10h for the T2, T3, and T4 configurations, respectively. For example, in the T_4 configuration with

H/Y=0.65, the DSTR of NRVC=12, NRVC=10, NRVC=7, and NRVC=4 was 0.12, 0.20, 0.25, and 0.36, respectively. When comparing the R1, R2, R3, and R4 configurations, the R4 configuration produces less sediment than the others. The DSTRs of the R1, R2, R3, and R4 configurations were 0.53, 0.38, 0.20, and 0.12, respectively, in the H/Y=0.65 with NRVC=4. This implies that forest cover density increases as longitudinal and transverse distances decrease. When the vegetation cover density increases, the sedimentation rate can be significantly reduced.

The performance of T_1, T_2, T_3, and T_4 demonstrates that the T_4 configuration is more effective at reducing sediment rate than the other configurations. The DSTR of T_1, T_2, T_3, and T_4 configurations was 0.42, 0.28, 0.25, and 0.11 in the H/Y=0.65 with NRVC=4, respectively.

The rectangular and triangular layouts indicated that the triangular layout performed better in reducing DSTR than the rectangular layout. For the NRVC=5, the DSTR of the H/Y=0.65, H/Y=0.90, and H/Y=1.2 in rectangular layout was 0.39, 0.41, and 0.42, respectively. For the NRVC=5, the DSTR of the H/Y=0.65, H/Y=0.90, and H/Y=1.2 in the triangular layout were 0.28, 0.37, and 0.41, respectively. The triangular configuration increased drag force and force-resisting area, slowing sediment transport.

Figure 10i shows the sediment transport rate versus coastal forest cover density. It was observed that the increasing density resulted in a significant decrease in the sediment transport rate. The sediment transport rate varied between 14 and 141 cm^3/s. It means that as forest cover density increases, the sediment transport rate decreases by 90%. The findings of this study corroborated those of previous researches. According to Jalil-Masir et al. [1, 43], the triangular layout performed better than the rectangular layout. Additionally, they reported that sediment transport rate decreased as forest cover density increased. Moreover, Parnak et al. stated that vegetation covers reduced sediment transport by 70% [9].

From the obtained results, the following points infer:

1) Various vegetation layouts consisting of triangular and rectangular layouts result in different effects on the capability of the sediment transfer rate (SDR).

2) The triangular layout is more efficient than the rectangular one due to its larger contact surface area with the flow.

3- Determining input model parameters is crucial in predicting the sediment transfer rate. However, the wave height and wave velocity significantly affect the sediment transfer rate (STR) capacity in a significant way.

4- Vegetation layout is not only limited to the rectangular and triangular types. Future studies can also investigate other vegetation layout types such as random layout, zigzag layout, etc.

5- The consequences of the ensemble model reveal that using outputs of several individual models in the structure of an ensemble model may remarkably enhance the result accuracy.

6- Combining the GMDH model with optimized algorithms was a drastic method to improve the GMDH results accuracy exactness.

7- Each optimized GMDH model had distinct accuracy because of dissimilar optimizing algorithms patterns.

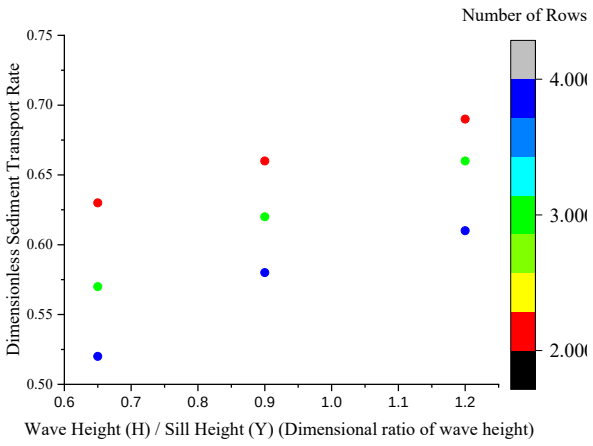

(a) (number of rows:2,3 ,and 4)

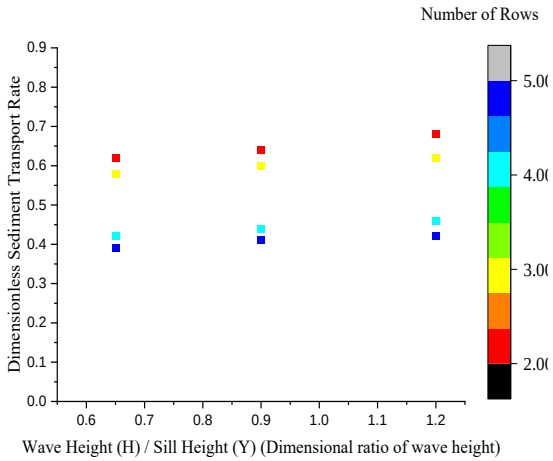

b (number of rows:2,3, 4, and 5)

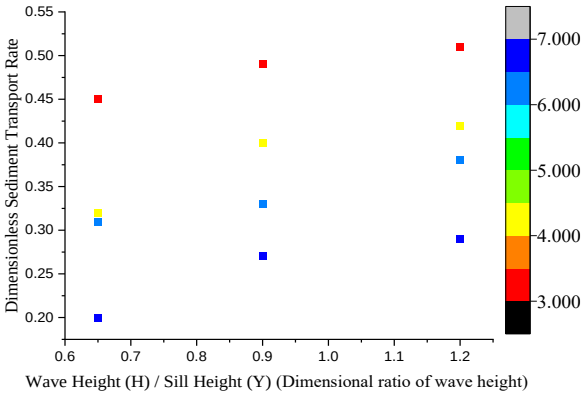

(c) (number of rows:7,6, 4, and 3)

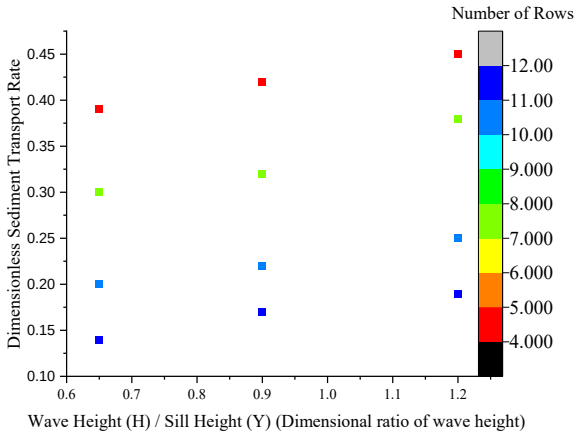

(d) (number of rows:13, 10, 7, and 4)

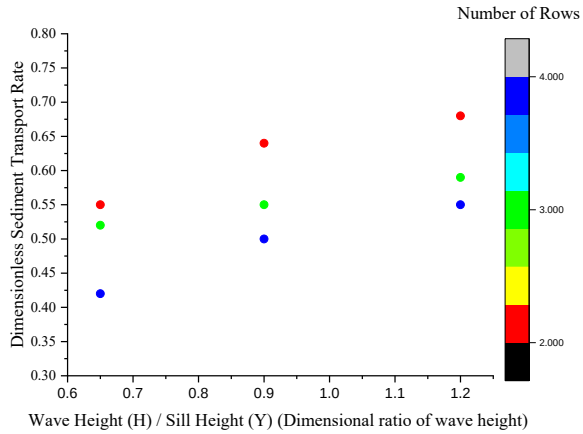

(g) (number of rows:2,3 ,and 4

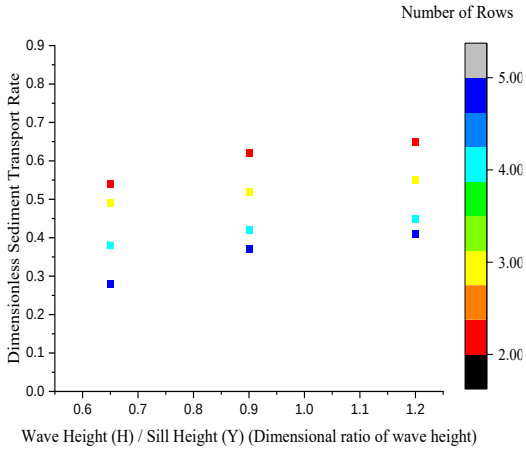

(h) (number of rows:2,3, 4, and 5)

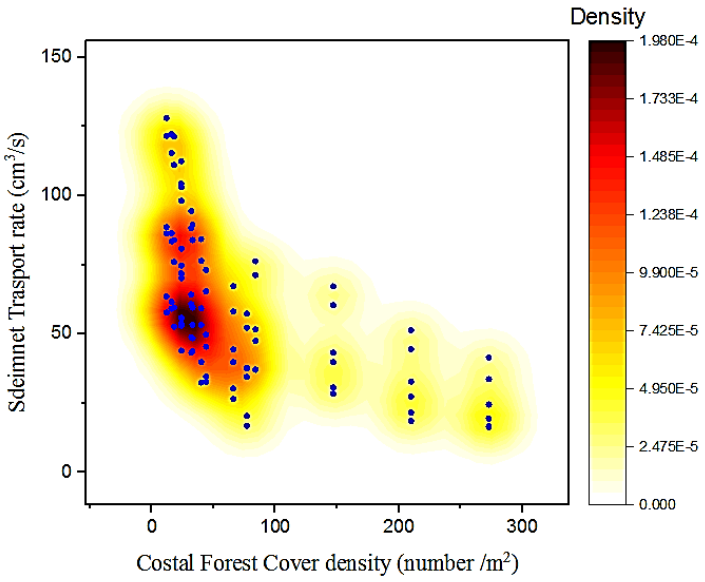

(i)

Figure 10. (a-d) The variation of sediment transport rate versus height wave for a: R_1 configuration, b: R_2 configuration, c: R_3 configuration, d: R_4 configuration
(e-h). The variation of sediment transport rate versus height wave in triangular layout for e: T_1 configuration, f: T_2 configuration, g: T_3 configuration, h: T_4 configuration
(i) (Variation of sediment transport rate versus the cover density)

4. Conclusion

Predicting sediment transport rates is critical for environmental pollution reduction. Decision-makers require robust models for predicting sediment transport rates in coastal regions. The coastal forest is one method for reducing the rate of sediment transport. The effect of coastal forests on sediment transport was investigated in this study through a comprehensive experiment. Additionally, the sediment transport rate was predicted using various soft computing models. The present study made several innovations, such as introducing a new ensemble model for predicting sediment transport, developing new optimization algorithms for training GMDH models, and investigating the effect of various parameters on sediment transport rate.

The inputs were the diameters of the sediments, stem diameter, cover density, wave height, wave velocity, cover height, and wave force. The HBA, RSOA, SCA, and PSOA were used to enhance the performance of the GMDH models. The current study predicted the sediment transport rate using an IMM model based on the outputs of GMDH models. This model took advantage of the strengths of multiple GMDH models. The MAE of the IMM was 0.145 m3/s, while the MAEs of the GMDH-HBA, GMDH-RSOA, GMDH-SCA, GMDH-PSOA, and GMDH in the testing level were 0.176 m^3/s, 0.312 m^3/s, 0.367 m^3/s, 0.498 m^3/s, and 0.612 m^3/s, respectively. The NSE of IMM, GMDH-HBA, GMDH-RSOA, GMDH-SCA, GMDH-PSOA, and GHMDH were determined to be 0.95, 0.93, 0.89, 0.86, 0.82, and 0.76, respectively.

The study of the effect of forest cover on sediment transport rates revealed that coastal forecast cover was critical in reducing wave height and sediment transport rates. Furthermore, as the number of rows of forest cover increased, sediment transport decreased. The experiment utilized a variety of configurations. The triangular layout was more effective at reducing sediment transport than the rectangular layout. This study can be expanded upon for future research. Other soft computing models, such as different types of artificial neural networks and optimization algorithms, can be used to forecast sediment transport. Moreover, the following studies can consider the effect of input uncertainty on sediment transport prediction. The current study's IMM model can be used to predict sediment transport rate and other variables such as temperature and streamflow.

List of abbreviations

Adaptive neuro-fuzzy inference system :(ANFIS)
Artificial neural network: (ANN)
Different coastal forest cover densities :(CFC)
Dimensionless sediment transport rate: (DSTR)
Genetic algorithm: (GA)
Inclusive multiple model :(IMM)
Mean absolute error: (MAE)
Particle swarm optimization: (PSO)
Percent bias: (PBIAS)
Nash–Sutcliffe model efficiency: (NSE)
Root mean square error: (RMSE)
Sediment transfer rate: (STR)
Group method of data handling: (GMDH)
Honey Badger algorithm: (HBA)
Sine cosine algorithm: (SCA)
Rat swarm optimization algorithm: (RSOA)
Particle swarm optimization algorithm: (PSOA)

5. References

1) Jalil-Masir, H., Fattahi, R., Ghanbari-Adivi, E., & Aghbolaghi, M. A. (2021a). Effects of different forest cover configurations on reducing the solitary wave-induced total sediment transport in coastal areas: An experimental study. Ocean Engineering, 235, 109350.
2) Cui, H., Zhou, J., Li, Z., & Gu, C. (2021). Soil and Sediment Pollution, Processes and Remediation. Frontiers in Environmental Science, 651.
3) Jalil-Masir, H., Fattahi, R., Ghanbari-Adivi, E., Asadi Aghbolaghi, M., Ehteram, M., Ahmed, A. N., & El-Shafie, A. (2022). An inclusive multiple model for predicting total sediment transport rate in the presence of coastal vegetation cover based on optimized kernel extreme learning models. *Environmental Science and Pollution Research*, *29*(44), 67180-67213.
4) da Silva, Y. J. A. B., Cantalice, J. R. B., Singh, V. P., Cruz, C. M. C. A., & da Silva Souza, W. L. (2016). Sediment transport under the presence and absence of emergent vegetation in a natural alluvial channel from Brazil. *International Journal of Sediment Research*, *31*(4), 360-367.
5) Zhang, Z., Chai, J., Li, Z., Chen, L., Yu, K., Yang, Z., ... & Zhao, Y. (2022). Effect of Check Dam on Sediment Load Under Vegetation Restoration in the Hekou-Longmen Region of the Yellow River. Frontiers in Environmental Science, 713.
6) Wang, H., Tang, H. W., Zhao, H. Q., Zhao, X. Y., & Lü, S. Q. (2015). Incipient motion of sediment in presence of submerged flexible vegetation. Water Science and Engineering. https://doi.org/10.1016/j.wse.2015.01.002
7) Chen, Y., Li, Y., Thompson, C., Wang, X., Cai, T., & Chang, Y. (2018). Differential sediment trapping abilities of mangrove and saltmarsh vegetation in a subtropical estuary. Geomorphology. https://doi.org/10.1016/j.geomorph.2018.06.018
8) Permatasari, I., Dewiyanti, I., Purnawan, S., Yuni, S. M., Irham, M., & Setiawan, I. (2018). The correlation between mangrove density and suspended sediment transport in Lamreh Estuary, Mesjid Raya Subdistrict, Aceh Besar, Indonesia. IOP Conference

Series: Earth and Environmental Science. https://doi.org/10.1088/1755-1315/216/1/012004
9) Parnak, F., Rahimpour, M., & Qaderi, K. (2018). Experimental investigation of the effect of rigid and flexible vegetation on sediment transport in open channels. Journal of Water and Soil, 32(2).
10) Mu, H., Yu, X., Fu, S., Yu, B., Liu, Y., & Zhang, G. (2019). Effect of stem basal cover on the sediment transport capacity of overland flows. Geoderma. https://doi.org/10.1016/j.geoderma.2018.09.055
11) Kusumoto, S., Imai, K., Gusman, A. R., & Satake, K. (2020). Reduction effect of tsunami sediment transport by a coastal forest: Numerical simulation of the 2011 Tohoku tsunami on the Sendai Plain, Japan. *Sedimentary Geology*. https://doi.org/10.1016/j.sedgeo.2020.105740
12) Sun, P., Wu, Y., Gao, J., Yao, Y., Zhao, F., Lei, X., & Qiu, L. (2020). Shifts of sediment transport regime caused by ecological restoration in the Middle Yellow River Basin. *Science of the Total Environment*. https://doi.org/10.1016/j.scitotenv.2019.134261
13) Liang, G., Panahi, F., Ahmed, A. N., Ehteram, M., Band, S. S., & Elshafie, A. (2021). Predicting municipal solid waste using a coupled artificial neural network with archimedes optimisation algorithm and socioeconomic components. Journal of Cleaner Production. https://doi.org/10.1016/j.jclepro.2021.128039
14) Panahi, F., Ehteram, M., Ahmed, A. N., Huang, Y. F., Mosavi, A., & El-Shafie, A. (2021). Streamflow prediction with large climate indices using several hybrid multilayer perceptrons and copula Bayesian model averaging. Ecological Indicators, 133, 108285.
15) Dodangeh, E., Panahi, M., Rezaie, F., Lee, S., Tien Bui, D., Lee, C. W., & Pradhan, B. (2020). Novel hybrid intelligence models for flood-susceptibility prediction: Meta optimization of the GMDH and SVR models with the genetic algorithm and harmony search. Journal of Hydrology. https://doi.org/10.1016/j.jhydrol.2020.125423
16) Moosavi, V., Mahjoobi, J., & Hayatzadeh, M. (2021). Combining Group Method of Data Handling with Signal Processing Approaches to Improve Accuracy of Groundwater Level Modeling. Natural Resources Research. https://doi.org/10.1007/s11053-020-09799-w
17) Aghelpour, P., & Varshavian, V. (2020). Evaluation of stochastic and artificial intelligence models in modeling and predicting of river daily flow time series. Stochastic Environmental Research and Risk Assessment. https://doi.org/10.1007/s00477-019-01761-4
18) Adnan, R. M., Liang, Z., Parmar, K. S., Soni, K., & Kisi, O. (2021). Modeling monthly streamflow in mountainous basin by MARS, GMDH-NN and DENFIS using hydroclimatic data. Neural Computing and Applications. https://doi.org/10.1007/s00521-020-05164-3
19) Mulashani, A. K., Shen, C., Nkurlu, B. M., Mkono, C. N., & Kawamala, M. (2022). Enhanced group method of data handling (GMDH) for permeability prediction based on the modified Levenberg Marquardt technique from well log data. *Energy*, *239*, 121915.
20) Panahi, M., Rahmati, O., Rezaie, F., Lee, S., Mohammadi, F., & Conoscenti, C. (2022). Application of the group method of data handling (GMDH) approach for landslide susceptibility zonation using readily available spatial covariates. *Catena*, *208*, 105779.
21) Ab. Ghani, A., Azamathulla, H.M., 2014. Development of GEP-based functional relationship for sediment transport in tropical rivers. Neural Comput. Appl. https://doi.org/10.1007/s00521-012-1222-9
22) Kitsikoudis, V., Sidiropoulos, E., & Hrissanthou, V. (2015). Assessment of sediment transport approaches for sand-bed rivers by means of machine learning. *Hydrological sciences journal*, *60*(9), 1566-1586.
23) Ebtehaj, I., Bonakdari, H., 2016. A comparative study of extreme learning machines and support vector machines in prediction of sediment transport in open channels. Int. J. Eng. Trans. B Appl. https://doi.org/10.5829/idosi.ije.2016.29.11b.03
24) Ebtehaj, I., Bonakdari, H., 2016. Bed load sediment transport estimation in a clean pipe using multilayer perceptron with different training algorithms. KSCE J. Civ. Eng. https://doi.org/10.1007/s12205-015-0630-7
25) Roushangar, K., & Ghasempour, R. (2017). Prediction of non-cohesive sediment transport in circular channels in deposition and limit of deposition states using SVM. *Water Science and Technology: Water Supply*, *17*(2), 537-551.
26) Riahi-Madvar, H., & Seifi, A. (2018). Uncertainty analysis in bed load transport prediction of gravel bed rivers by ANN and ANFIS. *Arabian Journal of Geosciences*, *11*(21), 688.
27) Baniya, M.B., Asaeda, T., Shivaram, K.C., Jayashanka, S.M.D.H., 2019. Hydraulic parameters for sediment transport and prediction of suspended sediment for Kali Gandaki River basin, Himalaya, Nepal. Water (Switzerland). https://doi.org/10.3390/w11061229
28) Kargar, K., Safari, M. J. S., Mohammadi, M., & Samadianfard, S. (2019). Sediment transport modeling in open channels using neuro-fuzzy and gene expression programming techniques. *Water Science and Technology*, *79*(12), 2318-2327.
29) Wang, G. G., Deb, S., & Cui, Z. (2019). Monarch butterfly optimization. *Neural computing and applications*, *31*(7), 1995-2014.

30) Li, S., Chen, H., Wang, M., Heidari, A. A., & Mirjalili, S. (2020). Slime mould algorithm: A new method for stochastic optimization. Future Generation Computer Systems, 111, 300-323.
31) Wang, G. G. (2018). Moth search algorithm: a bio-inspired metaheuristic algorithm for global optimization problems. *Memetic Computing*, *10*(2), 151-164.
32) Yang, Y., Chen, H., Heidari, A. A., & Gandomi, A. H. (2021). Hunger games search: Visions, conception, implementation, deep analysis, perspectives, and towards performance shifts. *Expert Systems with Applications*, *177*, 114864. https://doi.org/10.1016/j.eswa.2021.114864
33) Ahmadianfar, I., Heidari, A. A., Gandomi, A. H., Chu, X., & Chen, H. (2021). RUN beyond the metaphor: an efficient optimization algorithm based on Runge Kutta method. *Expert Systems with Applications*, *181*, 115079.
34) Radaideh, M. I., & Kozlowski, T. (2020). Analyzing nuclear reactor simulation data and uncertainty with the group method of data handling. Nuclear Engineering and Technology. https://doi.org/10.1016/j.net.2019.07.023
35) Hashim, F. A., Houssein, E. H., Hussain, K., Mabrouk, M. S., & Al-Atabany, W. (2022). Honey Badger Algorithm: New metaheuristic algorithm for solving optimization problems. *Mathematics and Computers in Simulation*, *192*, 84-110.
36) Dhiman, G., Garg, M., Nagar, A., Kumar, V., & Dehghani, M. (2021). A novel algorithm for global optimization: rat swarm optimizer. *Journal of Ambient Intelligence and Humanized Computing*, *12*, 8457-8482.
37) Mirjalili, S. (2016). SCA: A Sine Cosine Algorithm for solving optimization problems. Knowledge-Based Systems. https://doi.org/10.1016/j.knosys.2015.12.022
38) Abualigah, L., & Diabat, A. (2021). Advances in Sine Cosine Algorithm: A comprehensive survey. Artificial Intelligence Review. https://doi.org/10.1007/s10462-020-09909-3
39) Achite, M., Banadkooki, F. B., Ehteram, M., Bouharira, A., Ahmed, A. N., & Elshafie, A. (2022). Exploring Bayesian model averaging with multiple ANNs for meteorological drought forecasts. Stochastic Environmental Research and Risk Assessment, 1-26.
40) Ehteram, M., Ahmed, A. N., Kumar, P., Sherif, M., & El-Shafie, A. (2021). Predicting freshwater production and energy consumption in a seawater greenhouse based on ensemble frameworks using optimized multi-layer perceptron. *Energy Reports*, *7*, 6308-6326.
41) Rezapooran, A., & Fattahi, R. (2023). Performance Comparison of Hybrid Protection Methods in Weakening coast Waves. *International Journal of Maritime Technology*, *17*, 1-12.
42) Mirzakhani, G., Ghanbari-Adivi, E., & Fattahi, R. (2023). Sediment trapping efficiency in different coastal forest characteristics. Arabian Journal of Geosciences, 16(9), 502
43) Jalil Masir, H., Fattahi, R., Ghanbari Adivi, E., & Asadi Aghbolaghi, M. (2021b). Experimental investigation on impact of the coastal Forest on reducing sediment transport rate at littoral Zone. Irrigation and Water Engineering, 11(4), 38-52.
44) Bazrafshan, O., Ehteram, M., Latif, S. D., Huang, Y. F., Teo, F. Y., Ahmed, A. N., & El-Shafie, A. (2022). Predicting crop yields using a new robust Bayesian averaging model based on multiple hybrid ANFIS and MLP models. *Ain Shams Engineering Journal*, *13*(5), 101724.